Design of hydrazide-bearing HDACIs based on panobinostat and their p53 and FLT3-ITD dependency in anti-leukemia activity

Xiaoyang Li[1,2,#,*], **Yuqi Jiang**[1,#], **Yuri K. Peterson**[2], **Tongqiang Xu**[1], **Richard A. Himes**[3], **Xin Luo**[4], **Guilin Yin**[4], **Elizabeth S. Inks**[2], **Nathan Dolloff**[5], **Stephanie Halene**[6], **Sherine S.L. Chan**[2], **C. James Chou**[2,*]

[1]Ocean University of China, School of Medicine and Pharmacy, Qingdao, Shandong, 266071, China

[2]Department of Drug Discovery and Biomedical Sciences, College of Pharmacy, Medical University of South Carolina, Charleston, South Carolina 29425, USA

[3]Department of Chemistry and Biochemistry, College of Charleston, 66 George Street, Charleston, South Carolina 29424, USA

[4]Technology Center of Qingdao Customs, Qingdao, Shandong, 266002, China

[5]Department of Cellular and Molecular Pharmacology & Experimental Therapeutics, Medical University of South Carolina, Charleston, SC29425, USA

[6]Section of Hematology, Department of Internal Medicine and Yale Cancer Center, Yale University School of Medicine, New Haven, CT 06511, USA.

Abstract

Here we present a new series of hydrazide-bearing class I selective HDAC inhibitors designed based on panobinostat. The cap, linker, and zinc-binding group were derivatized to improve HDAC affinity and anti-leukemia efficacy. Lead inhibitor **13a** shows picomolar or low nanomolar IC_{50} against HDAC1 and HDAC3 and exhibits differential toxicity profiles toward multiple cancer cells with different FLT3 and p53 status. **13a** indirectly inhibits the FLT3 signaling pathway and down-regulates the master anti-apoptotic proteins, resulting in the activation of pro-caspase3 in in wt-p53 FLT3-ITD MV4–11 cells. While in the wt-FLT3 and p53-null cells, **13a** is incapable of causing apoptosis at therapeutic concentration. The MDM2 antagonist and the proteasome

[*]**Corresponding Authors:** C.J.C.: Phone: 843-792-1289. Fax: 843-792-1617. chouc@musc.edu; X. L.: lixiaoyang@ouc.edu.cn.
[#]These two authors contributed equally.

inhibitor promote **13a**-triggered apoptosis by preventing p53 degradation. Furthermore, we demonstrate that apoptosis rather than autophagy is the key contributing factor for **13a**-triggered cell death. When compared to panobinostat, **13a** is not mutagenic and displays superior *in vivo* bioavailability and higher $AUC_{0\text{-inf}}$.

Graphical Abstract
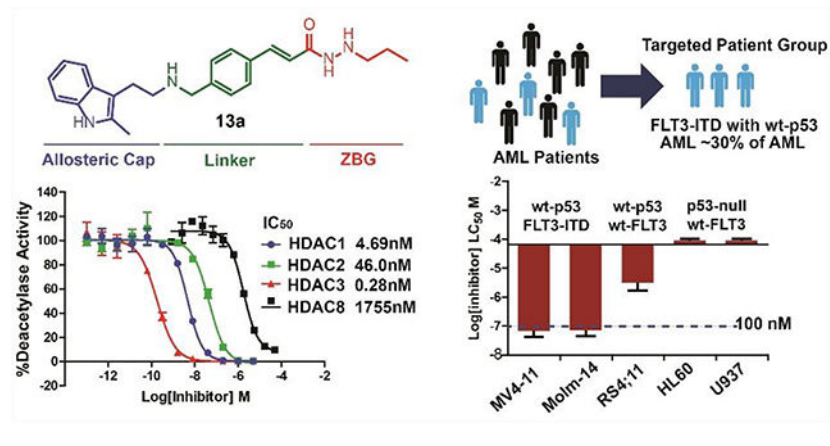
Introduction

Acute myelogenous leukemia (AML) is characterized by the uncontrolled proliferation and survival of immature malignant myeloid cells in parallel with the concurrent loss of normal hematopoiesis.[1–2] The standard anti-AML therapies since 1973 are based on cytotoxic chemotherapy using antimetabolites such as cytarabine (ara-C), and the DNA intercalating anthracyclines such as daunorubicin or idarubicin.[3] Although a series of targeted drugs including FLT3 inhibitors, IDH2 inhibitors, and Bcl-2 inhibitors have been approved for the treatment of AML, their uses limit specific patient population and undergo a high possibility of clonal resistance.[4–5] Three-quarters of all AML patients are > 60 years of age, only less than 10% of them achieve disease-free survival greater than 5 years.[5] With an increase in life expectancy in the U.S., AML cases are expected to become more prevalent, and there is a need for more effective and better-tolerated therapies.[6]

Unlike chronic myelogenous leukemia (CML), which is characterized by a more uniform genetic abnormality and a reciprocal translocation of the BCR and ABL genes,[7] AML has various cytogenetic abnormalities and mutations, such as FLT3, NPM1, c-kit tyrosine kinase and Ras mutations.[8–15] These constitutively active kinases initiate multiple pro-growth and pro-survival signaling through the mitogen-activated protein kinase/extracellular signal-regulated kinase (MAPK/ERK), signal transducer and activator of transcription 5 (STAT5), and PI3K/Akt kinase family mediated pathways and confer poor prognosis in AML.[8–9, 16–19] These genetic aberrations are not mutually exclusive and commonly coexist in AML cells.[20] Thus, the biggest challenge is to develop pharmacologic agents that possess significant specificity, yet are capable of attenuating multiple oncogenic signals in AML.

Class I HDACs play a crucial role in the transformation and survival of myeloid and lymphoid malignancies.[21–23] Inhibition or co-depletion of HDACs 1 and 2 elicits pro-apoptotic responses in leukemia.[22] HDAC3 activity is required for the initiation of leukemogenesis in acute leukemia.[24] Relevant to cancer therapy, HDAC3 depletion or inhibition significantly reduces proliferation and promotes differentiation in leukemia.[22] In our previous study, we demonstrated that our HDAC1, 2, and 3 selective inhibitors cause apoptosis in the AML cell line MV4–11, and displayed low nano-molar EC_{50}, which suggests that class I HDACs 1, 2, and 3 are potential molecular targets for the treatment of AML.[25–26]

The mechanisms of HDACIs lethality against leukemia and other cancer types can be elucidated as follows: 1) HDACIs activate the endogenous cyclin-dependent kinase (CDK) inhibitor p21[27] and disrupt cell cycle (especially mitotic spindle assembly) checkpoints;[28–29] 2) HDACIs activate both the intrinsic (mitochondrial) and extrinsic (death receptor-mediated) pathways of apoptosis by down-regulating the anti-apoptotic proteins such as X-linked inhibitor of apoptosis (XIAP) and cellular FLICE-like inhibitory protein (c-FLIP),[30–32] while up-regulating the pro-apoptotic proteins (Bim, Bmf and Noxa) through acetylation of p53[33–34] and inducing Bid cleavage;[35] 3) induction of autophagy by HDACIs through acetylation of the autophagy signaling component including Atg3[36] and regulation of mammalian target of rapamycin (mTOR) pathway.[37]

The actions of HDACIs in cancer cells reveal that in addition to epigenetic modifications, HDACs also control cell proliferation, differentiation, migration, and death by modification of non-histone proteins.[38] The tumor suppressor p53 is the first characterized example of non-histone protein acetylation.[39] It plays an important role in cellular signaling and stress responses and can either positively or negatively regulate apoptosis, cell cycle arrest, and autophagy.[40] P53 regulates apoptosis through control of transcription of pro-apoptotic members of the Bcl-2 family, including Bax, Puma, Noxa, and Bid.[41] P53 transcriptionally activates the endogenous CDK inhibitor p21, which can in turn inhibit cyclin E(A)/CDK2 and preserve the association of the tumor suppressor retinoblastoma protein.[42] Additionally, damage-regulated autophagy modulator (DRAM) that modulates autophagosome formation is also activated by p53.[37, 43]

Four HDACIs have been approved by the FDA: vorinostat,[44] romidepsin,[45] belinostat[46] and panobinostat,[47] among these, panobinostat is the most potent HDACI *in vitro* and *in vivo*. Structural regions and pharmacophore models of HDACIs contain three critical parts: a cap group (interacts with the surface of the enzyme), a linker (occupies the long hydrophobic tunnel), and a zinc-binding group (ZBG, functioning within the catalytic site).[48–49] Although hydroxamic acid is the most commonly used ZBG, it has disadvantages in its structural instability, lack of isoform selectivity, and the hydroxamic acid ZBG is mutagenic. Hydrazide-based ZBG-HDACIs have emerged in recent years in exploring new ZBGs of HDACIs that confirms to the physiological substrate geometric.[25–26, 50–51] As a new motif for HDACIs, its potency, structural stability, and off-target toxicity all need to be addressed. In our previous studies, we have demonstrated HDAC inhibitory activity and superior stability of the hydrazide ZBG.[25–26] However, the potential genotoxicity is a remains an important question. In fact, the hydrazine/hydrazide motif was extensively used in the past in

anti-depressants as well as first line antituberculosis agents today best characterized by isocarboxazid and isoniazid for chronic diseases.[52–54] Therefore, the hydrazide motif is expected to be better tolerated *in vivo*. Here we will describe and discuss the discovery of hydrazide-bearing HDACIs based on the structure of panobinostat with the comparative chemical structural studies, detailed p53 and FLT3 dependent anti-tumor mechanisms of action studies in AML cells, and preliminary mutagenic and pharmacokinetic studies.

Results and discussion

Chemistry

Scheme 1 showed the synthesis of intermediates **6a**-**6c**, **10a**, and **10b**. Phenylhydrazine (**1**) and 5-chloropentan-2-one (**2**) afford 2-(2-methyl-1*H*-indol-3-yl)ethanamine (**3**). **3** was mixed with aldehyde **4a**-**4c**, NaBH₃CN and CH₃COOH in methanol to give **5a**-**5c**, respectively. Boc-protection of **5a**-**5c** got **6a**-**6c**. Similarly, compound **3**, **8a**, and **8b** were reacted with benzaldehyde, then NaBH₃CN was added to obtain **9a** and **9b**, respectively, which also converted to Boc-protected product **10a** and **10b**.

Synthesis of product **13a**-**13d** was shown in Scheme 2. **6a** connected with hydrazine monohydrate by TBTU-mediated amide formation afforded **11**. **11** was reacted with propionaldehyde or *N*-Boc-2-aminoacetaldehyde to get Schiff base, which was suffered by NaBH₃CN gave reductant product **12a** or **12b**, respectively. **12c** and **12d** were achieved by reaction of **11** with acrylonitrile or methyl acrylate in ethanol. Boc de-protection of **12a**-**12d** leading end products **13a**-**13d**, respectively.

6b, **6c**, and **10a** were refluxed with hydrazine monohydrate to get **14a**-**14c**, which was reacted with propionaldehyde in the presence of magnesium sulfate followed by a reduction with sodium cyanoborohydride in acidified methanol to give the desired **15a**-**15c** (Scheme 3). Boc de-protection by TFA afforded **16a**-**16c**.

Scheme 4 described the synthesis of **24a**-**24c**. **17** connected with **18** got amide **19**, **20** connected with **21** by Mitsunobu reaction afforded ether **22**. **23a**, **23b**, and **23c**, the hydrazine product of **9b**, **19** and **22** respectively, were treated with propionaldehyde followed by NaBH₃CN to get end product **24a**, **24b**, and **24c**.

6a connected with 1,1-dimethylhydrazine, pyrrolidin-1-amine, piperidin-1-amine or pyrazolidine by TBTU-mediated amide formation to get intermediates **25a**-**25c**, respectively, which suffered TFA to get rid of the Boc group achieved **26a**-**26c** (Scheme 5). **12a** reacted with ethanal, propanal, *n*-butanal, *n*-pentanal or *n*-hexanal, followed by the addition of NaBH₃CN provided tertiary amine **27a**-**27e**. The end products **28a**-**28e** were achieved by Boc deprotection (Scheme 5).

Intermediate **11** reacted with 3-Bromo-1-propanol to get the propanol di-substituent product **29**, which was treated with TFA to afford **30** (Scheme 6).

Compounds design

Panobinostat is a highly potent hydroxamic acid-bearing pan-HDACI among all of the clinical HDACIs with low nano-molar IC_{50}s against HDACs and cancer cells but with limited selectivity. Although hydroxamic acid is the most commonly used ZBG for HDACIs, it shows limitations in isoform-selectivity, which is hypothesized to cause greater side effects than more selective HDACIs. Further, hydroxamic acid also suffers from reduction, hydrolysis, and glucuronidation *in vivo*, leading to the rapid inactivation of HDACIs.[55] This structural instability is the main reason for the poor pharmacokinetic profiles (short $t_{1/2}$ and low C_{max} and bioavailability) of clinical hydroxamate HDACIs.[56–59] Therefore, the exploration of new ZBG motifs for HDACIs holds great interest. Initially, Wang and colleagues demonstrated a novel hydrazide-based HDACI with class I selectivity.[51] We have shown further that the hydrazide motif as a potential ZBG displayed allosteric inhibition kinetics and was impervious to glucuronidation,[25–26] indicating that hydrazide could be a preferable ZBG fragment with improved selectivity and *in vivo* stability. Most recently, Son *et al.* also demonstrated hydrazide with long chain can be used for the design of HDAC11 selective inhibitor.[50]

Therefore, we modify the hydroxamic acid group of panobinostat using hydrazide motifs. It should be noted that among all of the hydrazide-based HDAC inhibitor studies, only one single *N*-substituent at the hydrazide tail was explored.[25–26, 50–51] Here in this study, we first design compounds with di-*N*- substituent at the hydrazide tail (Figure 1, R_4 group). As modifications in the cap and linker groups can also generate changes in enzymatic activity and selectivity, we also incorporate different fragments in the cap and linker (Figure 1). These newly designed compounds are expected to have the following improvements: 1) selectivity against class I HDACs; 2) similar potency toward class I HDACs and anti-leukemia activity compared to the parent molecule panobinostat; 3) less toxicity and improved *in vivo* PK profiles.

In our previous studies, hydrazide compounds with a 3 carbon on the hydrazide motif exhibited excellent HDAC inhibitory activity.[25–26] Therefore, we initiated this study by designing compounds in series 1 (Table 1) with *N*'-propylacetohydrazide as their ZBG and with modifications of panobinostat in the cap and linker groups. In detail, direct modification of hydroximic acid of panobinostat with *N*'-propylacetohydrazide affords **13a**. While keeping the cap group and ZBG unchanged, substituting the linker group of **13a** with 1-ethyl-4-methylbenzene and 1-ethyl-3-methylbenzene results in **16a** and **16b**, respectively; modifying both cap and linker of **13a** affords **16c**, **24a**, **24b**, and **24c**. Compounds **12a**, **15a**, **15b**, and **15c** are the Boc-containing structures of **13a**, **16a**, **16b**, and **16c**, respectively. Recombinant HDACs 1, 2, 3, and 6 are used to screen the newly designed compounds. IC_{50} of **13a** for HDAC1, 2, and 3 are 5.17, 49.5 and 0.28 nM, respectively, while they do not show inhibition against HDAC6 up to 100,000 nM. This indicates that modification of panobinostat by replacing hydroxamic acid with *N*'-propylacetohydrazide maintains its inhibitory activity toward class I HDACs, as well as acquired selectivity between class I HDACs and HDAC6. The IC_{50} of **13a** is much lower than that of **16a** and **16b**; therefore, (*E*)-1-ethyl-4-(prop-1-en-1-yl)benzene of **13a** is the optimized linker. Compound **16a** with 2-methyl-3-propyl-1*H*-indole as cap group is much more potent than **16c** with an

ethylbenzene cap. Compounds **24a**, **24b**, and **24c** with modifications in both cap and linker groups all show weaker activity than **13a**. Compounds **12a**, **15a**, **15b**, and **15c** with a Boc group exhibit reduced (**12a**, **15b**, **15c**) or equivalent (**15a**) activity when compared with their relative compounds; therefore, a branched aliphatic cap group may not improve the HDAC inhibitory activity of compounds.

As HDACs 1, 2, and 3 also have significant differences in surface charges and anchor interactions with the binding site, we further modified the hydrazide anchor (R_3) group of **13a** with motifs of varying electronegativity (**13c** and **13d**) and ionization **13b** (Table 2). HDAC inhibitory activity shows that the newly designed **13b**-**13d** all display less potency and selectivity when compare with **13a**. We then designed compounds with di-*N*-substituted and cyclic hydrazide groups (**26a**-**26c**, **28a**-**28e**, **30**) based on the ZBG space size difference between HDACs 1, 2, and 3 which are expected to achieve improved activity and selectivity these compounds. IC_{50}s of compounds with cyclic hydrazide (**26b**-**26c**) are all > 2,000 nM, which indicates cyclized hydrazide is a weak ZBG. Although some of the di-*N*-substituted compounds (**28b** and **28e**) display selectivity for HDAC3 to some extent, their activity is at least 100 times lower than *N'*-propylacetohydrazide **13a**. Therefore, HDACIs with di-*N*-substituted and cyclized hydrazide groups all have much lower potency than those with a 3-carbon linker chain mono-substitution hydrazide. To the best of our knowledge, it is the first time we discuss the structure-activity relationship (SAR) study of di-*N*-substituted hydrazide based HDACIs. These conclusions are important in the design of hydrazide HDACIs.

MV4–11 is widely used for the biological evaluation of drugs targeting AML.[60–62] What's more, in our previous study, MV4–11 cells showed high sensitivity to our hydrazide HDACIs.[26] Therefore, we chose the MV4–11 cell line to screen the antiproliferative activity of representative compounds **13a**, **16a**, **16b**, and **16c** with different linker- and cap-structures, plus the HDAC3 selective compound **28b** (Table 3). Class I selective inhibitors entinostat, as well as pan-inhibitors vorinostat and panobinostat, were chosen as positive controls. Results show that compounds **13a**, **16a**, **16b**, and **16c** have similar selective profiles. **13a** has the strongest enzyme inhibitory activity and antiproliferative activity with an EC_{50} of 15.35 nM, which is much lower than that of vorinostat and entinostat and comparable to that of panobinostat. HDACIs **26a**, **26b**, **26c**, and **30**, with little HDAC inhibitory activity, also do not affect cell proliferation at 50 μM.

13a is slow-on/slow-off class I inhibitor

Enzymatic and cell-based assays indicate that **13a** is the most potent HDACI among all of the compounds we designed. Thus, we chose **13a** for further biological study. To assess the HDAC isozymes selectivity of **13a**, we determined its IC_{50} for the other Zn^{2+}-dependent HDACs (HDAC4, 5, 7, 8, and 9), and compared it with pan-HDAC inhibitor panobinostat, as well as class I selective inhibitor entinostat (Table 4). As there are no appropriate substrates for HDAC10 and HDAC11, inhibitory activity toward these two isotypes was not determined.[63] IC_{50}s of **13a** for class I HDAC1, 2, and 3 are 4.69, 46.0, and 0.28 nM, respectively, which is comparable to those of panobinostat. Compound **13a** displays micro-molar IC_{50} (1.75 μM) for HDAC8 and does not inhibit (up to 10 μM) HDAC4, 5, 6, 7, or 9; therefore, **13a** is an HDAC1, 2, and 3 selective inhibitor. Although panobinostat shows

nanomolar IC_{50} for all types of HDACs, its EC_{50} for MV4–11 cells (5.2 nM) is close to that of class I HDAC selective HDACI **13a** (15.35 nM). This indicates that **13a** achieves HDAC isoform selectivity while maintaining potent anti-leukemia activity. We also find that **13a** does not show any inhibition to two metalloproteases, APN, and MMP (supporting information Figure S4), and trypsin used for the HDAC assay. Therefore, the anti-tumor activity of **13a** comes from its inhibition toward HDACs rather than non-specific metalloprotease inhibition.

Enzyme kinetic studies were also performed for HDACs 1 and 3 (Figure 2A and B). It is interesting to note that **13a** displays a non-competitive enzyme inhibition for HDAC1 and a mixed mode of inhibition for HDAC3. To better understand the potential binding modes and patterns between HDAC1 and HDAC3, we tested **13a** in four conditions each by probing the competitive site (CS) and the allosteric site (AS) of HDAC1 and HDAC3 using computational docking. As shown using the free-energy calculation in the docking simulations (Figure 2C), there is very large discrimination between the high affinity AS for **13a** and the very low-affinity CS of **13a** in HDAC1, in silico binding mode also shows **13a** fails to chelate due to the geometric constraint of the indole cap group preventing ZBG chelation with the Zn metal ion at the CS (supporting information Figure S6). This might be the reason that **13a** exhibits the non-competitive inhibition against HDAC1. For HDAC3, **13a** has a high binding affinity for both AS and CS sites based on free-energy calculation (Figure 2C). Potential binding mode of **13a** with HDAC3 shows in the catalytic site, the top five docking poses all display a reasonable distance between ZBG and Zn metal ion (Figure 2D). These results are consistent with the kinetic studies that **13a** inhibits HDAC1 non-competitively, and **13a** has a mixed inhibition mode due to its interaction with both AS and CS of HDAC3.

Inhibition of HDACs by hydrazide compound **13a** is time-dependent (slow-on) as concentration-response curves shift and IC_{50} values change with enzyme-inhibitor pre-incubation time (Figure 3A). For example, the IC_{50} of **13a** for HDAC3 following 90 min pre-incubation is 0.17 nM, which is 3 times lower than IC_{50} measured after 10 min pre-incubation. However, panobinostat reaches a steady-state within 10 min pre-incubation, indicating classical fast-on binding (Figure 3A). We also studied the release profile of **13a** and panobinostat by western blot. MV4–11 cells were treated with **13a** or panobinostat for 3 h. The drugs were then washed out and the cells cultured for 30 min, 1 h, 3 h, and 6 h without drugs. The t = 0 min time point was collected immediately after 3 h incubation with drugs. Histone acetylation caused by **13a** does not decrease within 6 h (Figure 3B). Acetylation of histone H3 caused by panobinostat begins to decrease after 1 h, but persisted through 6 h (Figure 3B). Therefore, **13a** and panobinostat both display slow-off release kinetics for class I HDACs. Interestingly, the acetylation of tubulin caused by panobinostat completely disappears after 30 min (Figure 3B). Inhibition of HDAC6 leads to tubulin acetylation, so panobinostat exhibits fast-off release kinetics against HDAC6, which is different from the class I HDACs. **13a** does not increase the acetylation of tubulin (Figure 3B), which is in agreement with its isoform selectivity. Although our HDAC inhibitors display slow-off and likely irreversible inhibition, the potent inhibition of HDACs are likely required because non-substituted hydrazine and hydrazides with bulky, branched, and long-

chain acyl-groups are significantly less effective at inhibiting HDACs and cancer cell proliferation.[25–26, 64]

Anti-cancer activity of 13a is p53 and FLT3 status-dependent

In our previous study, we concluded hydrazide-based HDACI **13e** displayed different mechanisms in MV4–11 and PC-3 cells depending on their p53 status.[26] However, only two cell lines were used and we only showed a simple mechanism with the phenomenon of apoptosis and cell cycle arrest.[26] Therefore, in this study, we further verify this hypothesis by conducting experiments to determine 13a's GI_{50} (average growth inhibition concentration) and LC_{50} (average lethal concentration) in the NCI60 tumor cell lines via the National Cancer Institute therapeutics program (Table 5). GI_{50}s of **13a** in 60 cell lines range from 17.3–338 nM; however, **13a** does not induce cell death at these concentrations. **13a** only induces lethality in 10 of the 60 cell lines at concentrations under 10 μM, and LC_{50} values of **13a** towards 7 of the 10 lethality-sensitive cell lines are below 1 μM. Unlike **13a**, panobinostat induces death in 18 of the 60 cell lines under the concentration of 10 μM (Figure 4A), which indicates that **13a** has a more selective profile in the NCI 60 cell screen. Deeper analysis of the NCI 60 cell line screen revealed that 4 (NCI-H226, HCT116, LOX IMVI, and UACC-62) of the 7 most sensitive cell lines to **13a** are p53 wild type (wt-p53); the other three sensitive cell lines are p53 mutants. Notably, none of the p53-null cell lines display sensitivity to **13a** induced lethality. This result coincides with our previous hypothesis that the response of cancer cell lines to hydrazide inhibitor is related to the p53 status.

In AML, p53 mutations occur in only ~8% of de novo AML.[66–67] Interestingly, over-expression of wt-p53 is associated with FLT3-ITD mutations suggesting a potential therapeutic niche.[68] FLT3 is important for the development of the hematopoietic and activating mutations of FLT3, which is now recognized as the most common molecular abnormality in AML and other hematologic malignancies as well. Patients with this activating mutation were found to have an increased incidence of leukocytosis and a decreased overall survival (OS).[69] Therefore, we also checked the dependency of **13a** with FLT3 status in addition to p53.

We chose 6 different leukemia and multiple myeloma cell lines with different p53 and FLT3 status, including MV4–11 and Molm-14 cell lines with wt-p53 and FLT3-ITD, the RS4;11 cell line with wt-p53 and wt-FLT3, as well as U937 and HL60 cell lines with p53-null and wt-FLT3 to test our compounds using the NCI-60 screening methodology. Results show that the wt-p53 leukemia cell lines are more sensitive to **13a** than p53-null cell lines. Furthermore, **13a** can cause cell death in wt-p53 MV4–11, Molm-14, and RS4;11, but only inhibits proliferation of p53-null HL-60 and U937 (Figure 4B). Within the wt-p53 cell lines, FLT3-ITD MV4–11 and Molm-14 cell lines are highly sensitive to HDACI treatment with significantly lower LC_{50} than wt-FLT3 cell line RS4;11. Therefore, wt-p53 and FLT3-ITD cell lines have the highest sensitivity of the 6 cell lines tested. We also tested the effect of **13a** in primary wt-p53 AML cells (Figure 4C). **13a** is toxic in all three patients' cells with < 1 μM EC_{50}.

We then explored the anti-tumor mechanism of **13a** in cell lines with different p53 and FLT3 status, including wt-p53 FLT3-ITD cell line MV4–11 (Figure 5A), wt-p53 wt-FLT3 cell line RS4;11 (Figure 5C), p53-null wt-FLT3 cell line HL60 (Figure 5D) and wt-p53 FLT3-non-expression SR cell line (supporting information Figure S7). LP411 (50, 100, and 200 nM), panobinostat (100 nM), vorinostat (5000 nM) and entinostat (1000 nM and 5000 nM) were used as controls. LP411 (3b[25]) is the most potent hydrazide HDACI in our previous study. As p53 can function as a "master regulator" of the apoptotic program and FLT3-ITD potently activates the STAT5 pathway in contrast to wild-type FLT3 signaling,[70–72] **13a** may have different mechanisms in cell lines with different p53 and FLT3 status.

In wt-p53 FLT3-ITD cell line MV4–11, pro-caspase3 cleavage is observed for the treatments of **13a**, LP411, panobinostat, vorinostat, and entinostat (Figure 5A). As caspase3 is the apoptotic effector, apoptosis occurs after the treatment of all the compounds. In addition, **13a** and LP411 down-regulate FLT3 and STAT5. Overexpression of FLT3 leads to the stimulation of proliferation and inhibition of apoptosis in many primary samples of leukemia.[73–75] Activation of FLT3 potently activates the STAT5 pathway, which constitutively induces cyclin D1, c-myc, and serine/threonine kinases Pim-1 and Pim-2, leading to aberrant cell growth of leukemia cells.[71, 76–78] We observe that pERK is down-regulated by **13a**. Activation of FLT3 kinase and its downstream proliferative signaling Ras/MEK/ERK pathway can also accelerate cell growth.[79] Therefore, our HDAC inhibitors can indirectly inhibit the FLT3 pathway via the down-regulation of FLT3, STAT5, and pERK. Due to the important role played by FLT3 in the survival and proliferation of AML blasts, and the fact that FLT3 inhibitor midostaurin (Rydapt) is an FDA-approved targeted small molecule for the treatment of AML with FLT3-ITD mutation, our compounds are likely to have a promising therapeutic effect in the treatment of AML with FLT3 mutations. **13a** also causes degradation of master anti-apoptotic proteins c-Flip and XIAP, eventually leading to cell apoptosis (cleavage of pro-caspase3) (Figure 5A). c-FLIP isoforms are major anti-apoptotic proteins that suppress caspase 8 and 10 activations, and therefore prevent the downstream apoptosis cascade,[80] while XIAP can directly bind to and inhibit caspase3 and 7[81–82] as well as prevent caspase 9 from activating.[83] P21$^{WAF1/Cip1}$, a CDK inhibitor, is markedly up-regulated by **13a**, which may contribute **13a**'s anti-proliferative activity. Furthermore, LC3 degradation is also observed in wt-p53 MV4–11 cells (Figure 5A). A recent study showed that LC3-II (an LC3 phospholipid conjugate) accumulation is related to autophagy, and intra-autophagosomal LC3-II may be degraded by lysosomal hydrolase.[84] Therefore, we hypothesize that the degradation of LC3 after 24h treatment with **13a** might indicate activation of autophagy. In a time-chased western blot experiment (Figure 5B), LC3-II fluxes and accumulates within 12 h and is later degraded within 24 h. Based on the western results, both apoptosis and autophagy occur in wt-p53 MV4–11 cells.

In the wt-p53 and wt-FLT3 RS4;11 cell line, cleavage of pro-caspase3 is only observed at high dose **13a** (200 nM), panobinostat (100 nM) and vorinostat (5000 nM), which means that wt-FLT3 RS4;11 is less sensitive than FLT3-ITD MV4–11 (Figure 5C). Another obvious difference between these two cell lines with different FLT3 status is that STAT5 does not down-regulate with the treatment of **13a**. It has been described that the signaling mechanisms of FL3-ITD differed from those conferred by wt-FLT3. STAT5 activation was

part of the FLT3 signaling chain, and that STAT5 was constitutively active in FLT3-ITD cells, whereas FLT3 ligand (FL) did not induce STAT5 phosphorylation in wt-FLT3 cells.[85] These might be the reason that our compounds behave differently in the FLT3-ITD MV4–11 cells and the wt-FLT3 RS4;11 cells. LC3 degradation is also not observed in wt-FLT3 RS4;11 cells (Figure 5C). However, p21$^{WAF1/Cip1}$ is up-regulated by **13a** in RS4;11 cells. In p53-null wt-FLT3 HL60 cells, **13a** can result in the degradation of anti-apoptotic protein c-Flip and XIAP but is unable to trigger apoptosis as pro-caspase3 is not cleaved to its active form (Figure 5D). **13a** also induces p21 up-regulation in HL60 cells consistent with previous reports that the p21 up-regulation by HDACIs is independent of p53 status resulting in the cell-cycle arrest but not cell death.[26] Moreover, LC3 is not degraded in HL60 cells; therefore, **13a** is incapable of causing apoptosis and autophagy in p53-null HL60 cells. It must be noted that **13a** does not cause wt-p53 SR cell line death (Table 5); the western blot result of **13a** in SR cells is shown in supporting information Figure S7. Pro-caspase3 does not cleave after treatment of **13a** for 24h. Interestingly, **13a** can up-regulate pERK, which is down-regulated in the other 3 cell lines. Additionally, FLT3 is undetectable in the SR cell line. In summary, the effect of **13a** depends on the cellular p53 status, which controls the levels of anti-apoptotic proteins c-FLT and XIAP, and caspase-3 cleavage and activation. **13a** also controls the expression of FLT-3 affecting cellular pro-survival and proliferation signaling pERK and STAT5 pathways, especially in AML with oncogenic FLT3 mutations. In combination, AML cells with wt-p53 and FLT3-ITD are the most sensitive to **13a** treatment.

It is also interesting that an increase in Hsp70 levels is not observed for **13a** but was observed for SAHA and panobinostat treatments (Figures 5A and C). We determined that 17-AAG, an Hsp90 inhibitor that can up-regulate Hsp70,[86] antagonized with **13a** in anti-proliferation activity when used at lower concentrations (supporting information Figure S8). Hsp70 up-regulation contributes to chemo-resistance in cancer therapeutic development, [87–89] which suggests that **13a** can be a more sustainable therapy compared to the classical HDACIs.

Preventing p53 degradation promotes 13a-triggered apoptosis

We also observe that **13a** leads to a down-regulation of p53 in MV4–11 and RS4;11 cells. As MDM2 is also down-regulated (via p53 down-regulation) by **13a** (Figure 5A), we hypothesize that the p53 down-regulation is mainly due to proteasome degradation instead of acetylation or phosphorylation. To study the mechanism of p53 down-regulation, we treated MV4–11 cells with **13a** plus the MDM2-p53 antagonist RG7388 and the p53 reactivator PRIMA-1^{met} for 24 h. RG7388 prevented the binding of p53 and MDM2 and inhibited ubiquitin-mediated proteasome degradation of p53. PRIMA-1^{met} can reactivate p53 by binding to and modifying thiol groups in the central domain of the mutated protein, so we used it as a negative control, as it will not restore p53 in the wt-p53 MV4–11 cell line. RG7388 blocked p53 degradation caused by **13a**, thus promoting the cleavage of pro-caspase3 (Figure 6A). However, degradation of MDM2 caused by **13a** is not fully restored by RG7388. We speculate that this is because of the significant cell death after the 24 h treatment (Figure 6A). Therefore, we treated with **13a** and RG7388 for 3 h, 6 h, 9 h, 12 h, and 24 h, respectively, and then detected the level of p53 and MDM2. As expected, RG7388

fully blocks the degradation of p53 and MDM2 caused by **13a** within 12 h (Figure 6B). Similar results are also shown in T-PLL cells treated with panobinostat and MDM2-p53 antagonist or p53 reactivator.[90–91] Furthermore, **13a** and RG7388 synergistically inhibit cell proliferation (Figure 6C, CI < 0.9). Collectively, we conclude that the mechanism of p53 down-regulation is due to MDM2 activation and proteasome degradation, which is further confirmed via proteasome inhibitor. In Figure 7A, proteasome inhibitor bortezomib blocks the **13a**-induced p53 degradation. Treatment with **13a** in combination with bortezomib facilitates the cleavage of pro-caspase3 (Figure 7B), indicating that bortezomib can promote **13a**-triggered apoptosis. **13a** and bortezomib also synergistically inhibit cell proliferation (Figure 7C, CI < 0.9), which is consistent with the previous results in Figure 5.

Caspase inhibitor z-VAD inhibits MV4–11 death caused by 13a

As shown in Figure 5A and B, **13a** results in cell apoptosis and also triggers autophagy in wt-p53 MV4–11 cells. Apoptosis and autophagy) are two forms of programmed cell death, which is in contrast with the non-physiological necrotic process that occurs as a result of infection or injury.[92] To explore the mechanism of MV4–11 cell death, we treated MV4–11 cells with **13a** plus the pan-caspase inhibitor z-VAD and the autophagy inhibitors chloroquine or wortmannin for 24 h, and then measured cell viability (Figure 8A). Autophagy inhibitors chloroquine and wortmannin are incapable of attenuating cell death, while in the presence of pan-caspase inhibitor z-VAD, **13a**-triggered cell death was rescued. Western blots also indicated that among the three co-treatment agents with **13a**, z-VAD can prevent the cleavage of pro-caspase3, suggesting z-VAD can rescue cell death by inhibiting apoptosis (Figure 8B). The autophagy inhibitor chloroquine did block the degradation of LC3-II and prevent the progression of autophagy but it does not prevent **13a**-induced cell death (Figure 8B). Therefore, apoptosis is likely the main mechanism leading to **13a**-triggered cell death rather than lethal autophagy.

13a has favorable toleration and *in vivo* PK properties

As a potential clinical therapy, the inhibitor's efficacy and ability to influence targeted biomarkers must be validated *in vivo*. The chemical agent should be well tolerated with no overbearing toxicity and with optimized PK properties in addition to its pharmacological efficacy. We have already demonstrated the *in vitro* anti-tumor activity of **13a**. Our next step is to test its mutagenic toxicity and pharmacokinetic properties, two major limiting factors for HDACIs in the clinic. Mini-Ames tests were conducted to determine the mutagenic toxicity of **13a**, and mutagen 2-aminoanthracene and panobinostat were used as positive controls. **13a** is not mutagenic compared to the known mutagen 2-aminoanthracene and panobinostat (Figure 9), which suggests that **13a** bear less genotoxicity than panobinostat. We then conducted a pharmacokinetic study for **13a** by iv as well as oral administration and compared with panobinostat. The *in vivo* $t_{1/2}$ of **13a** iv and oral are 15.2 h and 7.45 h, which are significantly longer than panobinostat in mice (2.9 h oral). AUC_{0-inf} (ng·h/mL) of **13a** is 265 ng/mL at 20 mg/kg oral which is 2 times that of panobinostat 50 mg/kg oral (126 ng/mL) (Table 6).[93] What's more, the bioavailability of **13a** (19.8%) is much superior than that of panobinostat (4.62%).[93] Therefore, **13a** displays much more favorable PK profiles in mice. The slow-on/slow-off kinetics profile reveals that **13a** binds tightly and acts much

longer than the classical inhibitors, regardless of its actual $t_{1/2}$. This provides the possibility of using lower doses or longer intervals between dosing, which should minimize any potential adverse effects and make this a more effective and durable therapy than vorinostat and panobinostat.

Conclusion

We have designed and synthesized a new series of hydrazine-bearing class I selective HDACIs based on the modification of the three domains (cap, linker, and ZBG) of panobinostat. For the first time, we design di-*N*-substituents hydrazide based inhibitor and discuss their SAR. The representative compound **13a** exhibits potent activity against class I HDAC 1, 2, and 3, with IC_{50} values of 5.17 nM, 49.5 nM, and 0.28 nM, respectively. However, **13a** displays micromolar IC_{50} for HDAC8 and does not show inhibition up to 10 μM for HDACs 4, 5, 6, 7, and 9. Therefore, **13a** not only maintains panobinostat's potency toward class I HDACs and has HDACs 1, 2, and 3 selectivity. Interestingly, **13a** displays mixed binding mode to HDAC3, but a non-competitive binding to HDAC1, which could potentially be used to identify the allosteric site these hydrazide inhibitors targets. The EC_{50} of **13a** against wt-p53 MV4–11 cells is 15.35 nM, which is comparable to that of panobinostat (5.2 nM). As **13a** has differential activities in cell lines with different p53 and FLT3 status, we conducted a multitude of molecular biological experiments to reveal the anti-tumor mechanism in wt-p53 FLT3-ITD MV4–11 cell line, wt-p53 wt-FLT3 RS4;11 cell line, p53-null wt-FLT3 HL-60 cell line and wt-p53 FLT3-undetectable SR cell line together with LP41l (a comparable lead hydrazide HDACI), vorinostat, and panobinostat. In the wt-p53 FLT3-ITD MV4–11 cell line, **13a** indirectly inhibits the FLT3 signaling pathway via down-regulation of FLT3, STAT5, and pERK, making this compound a promising therapeutic strategy for the treatment of AML with FLT3 mutation. It also down-regulates master anti-apoptotic proteins c-Flip and XIAP as well as leads to cleavage of pro-caspase3. Also, in the wt-p53 and wt-FLT3 cell line RS4;11, **13a** cannot down-regulate activation of the STAT5 pathway, and this might be the main contributing factor for RS4;11 being less sensitive to the HDACI treatment. In addition, **13a** is incapable of causing apoptosis in p53-null HL60 cells as expected, indicating that a functional p53 is required for the selective toxicity. This hypothesis is further strengthened when p53-MDM2 antagonist RG7388 and proteasome inhibitor bortezomib are used to prevent the degradation of p53, resulting in effects with **13a** to induce cell death (CI from 0.5–0.9). All of these results reveal that **13a** displays selective class I HDAC inhibition, inducing targeted lethality against leukemia cell lines depending on their p53 status and FLT3 status. We conclude that FLT3-ITD cell lines are more sensitive than wt-FLT3 cell lines among cells with wt-p53, and **13a** displays wt-p53 and FLT3-ITD dependent anti-leukemia activity, which can be a potential therapeutic niche for AML and a useful diagnostic indication for patient selection in the clinic.

MV4–11 cell death caused by **13a** can be rescued by the pan-caspase inhibitor z-VAD, unlike the autophagy inhibitors chloroquine and wortmannin. This indicates that the mechanism of **13a**'s lethality against wt-p53 cells is apoptosis, rather than autophagy. Although compound **13a** shows slightly lower potency than panobinostat *in vitro*, it displays an HDAC class I selective profile. In addition, an increase in Hsp70 level is not observed for

13a but is observed for panobinostat and vorinostat (Figure 5A). As Hsp70 up-regulation has contributed to chemoresistance in cancer therapeutic development,[87–89] **13a** could be a more effective and durable therapy compared to panobinostat *in vivo*. **13a** is not mutagenic and showed superior bioavailability and half-life with a higher AUC exposure, and a longer $t_{1/2}$ *in vivo*, which suggests that it is likely to be a better therapeutic agent than panobinostat in the clinic. Furthermore, the slow-on/slow-off inhibition profile reveals that **13a** can tightly bind to HDACs, which makes them act much longer than classical inhibitors, despite the $t_{1/2}$, if its C_{max} reaches effective concentration. This provides the possibility of using lower doses or longer intervals between dosing.

Experimental Section

General chemistry

All solvents, reagents, and compound precursors were purchased from Sigma-Aldrich or other chemical vendors and used as received unless otherwise noted. NMR data were collected in deuterated solvents using a Bruker Nanobay 400 MHz instrument with TMS as an internal standard. Chemical shifts (δ) are given in parts per million, and coupling constants (J) are reported in hertz (Hz). Mass spectral data were gathered on a Thermo LCQ Fleet mass spectrometer using electrospray ionization. Purification was performed using a Teledyne Isco Combiflash 200 on prepacked C18-Aq columns. All target compounds were at least 95% pure as confirmed via UV detection of ESI-LCMS, performed on an Waters e2695 HPLC instrument using an XBridge C18 column (5 μm, 4.6 mm × 150 mm) using a gradient of water/methanol plus 0.1% formic acid (0–1 mins from 0–50% methanol, 1–12 mins from 50% to 100% methanol, 12–14 min to 0% methanol, and maintained at 0% for 1 minute).

Procedure for preparation of target compounds

2-(2-methyl-1*H*-indol-3-yl)ethanamine (3)—Phenyl hydrazine (**1**, 1.08 g, 10.0 mmol) was dissolved in absolute ethanol (50 mL), to this solution was added 5-chloropentan-2-one (**2**, 1.80 g, 15.0 mmol) dropwise, the mixed solution was refluxed at 80 °C for 4 h. After the reaction finished, volatiles were removed under vacuum and resulting residue was dissolved in DCM. The organic layer was washed with brine, dried over anhydrous $MgSO_4$ and evaporated under vacuum. The crude product was purified on reverse phase columns eluted with acetonitrile and water to yield pure product **3** (1.36 g, 80% yield). ^{1}H NMR (400 MHz, DMSO-d_6) δ 10.68 (s, 1H), 7.39 (d, $J = 7.7$ Hz, 1H), 7.21 (d, $J = 7.9$ Hz, 1H), 6.98 (t, $J = 7.2$ Hz, 1H), 6.92 (t, $J = 7.2$ Hz, 1H), 2.69 (s, 4H), 2.31 (s, 3H).

(*E*)-3-(4-(((2-(2-methyl-1*H*-indol-3-yl)ethyl)amino)methyl)phenyl)acrylic acid (5a)—Compound **3** (0.87 g, 5 mmol) was dissolved in 100 mL methanol, to this solution was added (*E*)-3-(4-formylphenyl)acrylic acid (**4a**, 0.88g, 5mmol), sodium cyanoborohydride (1.24 g, 20 mmol) and 2 drops of acetic acid. The mixture was allowed to stir overnight and volatiles were removed under vacuum. The crude product was purified on reverse phase columns eluted with acetonitrile and water to yield pure product **5a** (1.17g, 70% yield). ^{1}H NMR (400 MHz, DMSO-d_6) δ 10.69 (s, 1H), 7.57 (d, $J = 8.1$ Hz, 2H), 7.47 (d, $J = 16.0$ Hz, 1H), 7.38–7.35 (m, 3H), 7.21 (d, $J = 7.9$ Hz, 1H), 6.98–6.93 (m, 1H), 6.92–

6.86 (m, 1H), 6.50 (d, J = 16.0 Hz, 1H), 3.78 (s, 2H), 2.82 (t, J = 7.3 Hz, 2H), 2.70 (t, J = 7.4 Hz, 2H), 2.31 (s, 3H). ESI-MS m/z: 335.17 [M + H]$^+$.

Methyl 4-(((2-(2-methyl-1H-indol-3-yl)ethyl)amino)methyl)benzoate (5b)—Using the synthetic method of **5a**, compound **3** and **4b** gave **5b** as a white solid, 72% yield. ^{1}H NMR (400 MHz, DMSO-d_6) δ 10.81 (s, 1H), 7.99 (d, J = 8.2 Hz, 2H), 7.59 (d, J = 7.9 Hz, 2H), 7.40 (d, J = 7.7 Hz, 1H), 7.25 (d, J = 7.9 Hz, 1H), 7.01–6.91 (m, 2H), 4.12 (s, 2H), 3.86 (s, 3H), 2.92–2.88 (m, 4H), 2.32 (s, 3H). ESI-MS m/z: 323.08 [M + H]$^+$.

Methyl 3-(((2-(2-methyl-1H-indol-3-yl)ethyl)amino)methyl)benzoate (5c)—Using the synthetic method of **5a**, compound **3** and **4c** gave **5c** as a white solid, 70% yield. ^{1}H NMR (400 MHz, DMSO-d_6) δ 10.70 (s, 1H), 7.97 (s, 1H), 7.84 (d, J = 7.7 Hz, 1H), 7.62 (d, J = 7.6 Hz, 1H), 7.48 (t, J = 8.1 Hz, 1H), 7.37 (d, J = 7.7 Hz, 1H), 7.22 (d, J = 7.9 Hz, 1H), 6.98 (t, J = 7.3 Hz, 1H), 6.91 (t, J = 7.4 Hz, 1H), 3.86 (s, 3H), 3.82 (s, 2H), 2.83 (t, J = 7.5 Hz, 2H), 2.70 (t, J = 7.5 Hz, 2H), 2.31 (s, 3H). ESI-MS m/z: 323.17 [M + H]$^+$.

(*E*)-3-(4-(((tert-butoxycarbonyl)(2-(2-methyl-1H-indol-3 yl)ethyl)amino)methyl)phenyl)acrylic acid (6a)—Compound **5a** (0.67 g, 2 mmol) was dissolved in 15 mL 1 mol/L NaOH aqueous solution, to which was added 0.48 g (Boc)$_2$O and 2 mL THF. The mixture was stirred overnight and THF condensed under vacuum. The left NaOH aqueous solution was acidification by diluted hydrochloric acid and then was extracted by 20 mL ethyl estate for three times. The organic layer was washed by brine and dried over anhydrous MgSO$_4$. The solvent was evaporated under vacuum, the product was used for next step without purification. ^{1}H NMR (400 MHz, DMSO-d_6) δ 12.52 (s, 1H), 10.78 (s, 1H), 7.88–7.55 (m, 5H), 7.31–7.16 (m, 2H), 6.99–6.87 (m, 2H), 6.53 (d, J = 16.0 Hz, 1H), 4.49–4.31 (m, 2H), 3.27–3.20 (m, 2H), 2.79–2.73 (m, 2H), 2.27 (s, 3H), 1.38 (s, 9H). ESI-MS m/z: 435.17 [M + H]$^+$.

methyl 4-(((tert-butoxycarbonyl)(2-(2-methyl-1H-indol-3-yl)ethyl)amino)methyl)benzoate (6b)—Using the synthetic method of **6a**, compound **5b** gave **6b** as a white solid, 72% yield. ^{1}H NMR (400 MHz, CDCl$_3$) δ 7.96 (d, J = 8.1 Hz, 2H), 7.77 (s, 1H), 7.42–7.35 (m, 1H), 7.23 (t, J = 1.0 Hz, 1H), 7.16–7.14 (m, 1H), 7.11–7.02 (m, 2H), 4.56 (s, 1H), 4.23 (s, 1H), 3.89 (s, 3H), 3.42–3.30 (m, 2H), 2.94–2.84 (m, 2H), 2.37 (s, 3H), 1.48 (s, 9H). ESI-MS m/z: 423.17 [M + H]$^+$.

methyl 3-(((tert-butoxycarbonyl)(2-(2-methyl-1H-indol-3-yl)ethyl)amino)methyl)benzoate (6c)—Using the synthetic method of **6a**, compound **5c** gave **6c** as a white solid, 65% yield. ^{1}H NMR (400 MHz, DMSO-d_6) δ 10.71 (s, 1H), 7.88–7.86 (m, 2H), 7.52–7.50 (m, 2H), 7.40–7.30 (m, 1H), 7.22 (d, J = 7.8 Hz, 1H), 6.98 (t, J = 7.2 Hz, 1H), 6.91 (t, J = 7.5 Hz, 1H), 4.49–4.37 (m, 2H), 3.86 (s, 3H), 3.25 (t, J = 7.2 Hz, 2H), 2.78–2.74 (m, 2H), 2.27 (s, 3H), 1.37 (s, 9H). ESI-MS m/z: 423.17 [M + H]$^+$.

methyl 4-((benzylamino)methyl)benzoate (9a)—Using the synthetic method of **5a**, compound **7** and **8a** gave **9a** as a white solid, 72% yield. ^{1}H NMR (400 MHz, DMSO-d_6) δ 8.02 (d, J = 7.9 Hz, 2H), 7.63 (d, J = 7.9 Hz, 2H), 7.48–7.38 (m, 5H), 4.17 (s, 2H), 4.10 (s, 2H), 3.87 (s, 3H). ESI-MS m/z: 256.17 [M + H]$^+$.

methyl 4-(benzylamino)benzoate (9b)—Using the synthetic method of **5a**, compound **7** and **8b** gave **9b** as a white solid, 72% yield. ^{1}H NMR (400 MHz, DMSO-d_6) δ 7.67 (d, J = 8.8 Hz, 2H), 7.35–7.32 (m, 4H), 7.16 (t, J = 5.6 Hz, 1H), 6.62 (d, J = 8.8 Hz, 2H), 4.34 (d, J = 6.0 Hz, 2H), 3.73 (s, 3H). ESI-MS *m/z*: 323.08 [M + H]+. ESI-MS *m/z*: 242.08 [M + H]+.

methyl 4-((benzyl(tert-butoxycarbonyl)amino)methyl)benzoate (10a)—Using the synthetic method of **6a**, compound **9a** gave **10a** as a white solid, 75% yield. ^{1}H NMR (400 MHz, DMSO-d_6) δ 8.00 (d, J = 7.9 Hz, 2H), 7.61 (d, J = 7.9 Hz, 2H), 7.48–7.37 (m, 5H), 4.48–4.32 (m, 4H), 3.84 (s, 3H), 1.40 (s, 9H). ESI-MS *m/z*: 356.17 [M + H]+.

(E)-tert-butyl 4-(3-hydrazinyl-3-oxoprop-1-en-1-yl)benzyl(2-(2-methyl-1H-indol-3-yl)ethyl)carbamate (11)—To a solution of compound **6a** (0.86 g, 2 mmol) in DCM was added 2-(1H-benzotriazole-1-yl)-1,1,3,3-tetramethyluronium tetrafluoroborate (TBTU, 0.71 g, 2.4 mmol), followed by TEA (0.4 mL, 3 mmol). 30 mins later, hydrazine monohydrate (0.2 g, 4 mmol) was added. The reaction was allowed to stir overnight, and monitored by TLC. After the reaction finished, the solution of DCM was washed by brine and dried over anhydrous MgSO$_4$. Volatile was removed under vacuum, the residue was recrystallized by ethyl estate and hexane to yield a white solid **11** (0.44 g, 50% yield) was obtained on reverse phase columns eluted with acetonitrile and water. ^{1}H NMR (400 MHz, DMSO-d_6) δ 10.72 (s, 1H), 9.35 (s, 1H), 7.54 (d, J = 7.8 Hz, 2H), 7.45 (d, J = 16.0 Hz, 1H), 7.32–7.21 (m, 4H), 6.99 (t, J = 7.3 Hz, 1H), 6.92 (t, J = 7.3 Hz, 1H), 6.55 (d, J = 16.0 Hz, 1H), 4.47–4.31 (m, 4H), 3.25–3.21 (m, 2H), 2.79–2.76 (m, 2H), 2.27 (s, 3H), 1.37 (s, 9H). ESI-MS *m/z*: 449.17 [M + H]+.

(E)-tert-butyl (2-(2-methyl-1H-indol-3-yl)ethyl)(4-(3-oxo-3-(2-propylhydrazinyl)prop-1-en-1-yl)benzyl)carbamate (12a)—Compound **11** (0.45 g, 1 mmol) was dissolved in 20 mL ethanol followed by the addition of 1.2 g anhydrous MgSO$_4$ and propionaldehyde (0.07 g, 1.2 mmol). The reaction was monitored by TLC, after finished, MgSO$_4$ was filtered and ethanol was removed under vacuum. The resulting residue was dissolved in 20 mL methanol, to this solution was added 5 mg methyl orange and 0.31 g (5 mmol) sodium cyanoborohydride (NaBH$_3$CN). Mixture of methanol and concentrated hydrochloric acid (1:1) was added dropwise until the solution turned and stayed red. Six h later, volatiles were removed under vacuum and purified on reverse phase columns eluted with acetonitrile and water to yield pure product **12a** (0.29 g, 60% yield). ^{1}H NMR (400 MHz, DMSO-d_6) δ 10.67 (s, 1H), 9.67 (s, 1H), 7.53 (d, J = 8.0 Hz, 2H), 7.41 (d, J = 15.8 Hz, 1H), 7.29–7.24 (m, 2H), 7.21 (d, J = 7.9 Hz, 2H), 6.96 (t, J = 7.4 Hz, 1H), 6.89 (t, J = 7.0 Hz, 1H), 6.51 (d, J = 15.8 Hz, 1H), 5.03 (s, 1H), 4.39 (s, 1H), 4.27 (s, 1H), 3.21 (s, 2H), 2.76 (s, 2H), 2.68 (t, J = 7.0 Hz, 2H), 2.25 (s, 3H), 1.46–1.41 (m, 2H), 1.34 (s, 9H), 0.87 (t, J = 7.4 Hz, 3H). ^{13}C NMR (101 MHz, DMSO-d_6) δ 164.28, 155.53, 140.65, 138.63, 135.63, 134.25, 132.50, 128.65, 128.51, 128.09, 120.44, 120.39, 118.52, 117.48, 110.83, 107.47, 79.20, 53.55, 49.59, 47.39, 28.43, 23.30, 21.24, 12.01, 11.49. ESI-MS *m/z*: 491.25 [M + H]+. HRMS (AP-ESI) m/z calcd for C$_{29}$H$_{38}$N$_4$O$_3$ [M + H]+ 491.30167, found 491.30157.

(E)-2-(2-methyl-1H-indol-3-yl)-N-(4-(3-oxo-3-(2-propylhydrazinyl)prop-1-en-1-yl)benzyl)ethanaminium 2,2,2-trifluoroacetate (13a)—Compound **12a** (0.24 g, 0.5

mmol) was dissolved in 10 mL mixed solution of DCM and TFA (1:1), the solution was stirred at room temperature for 1 hour. The reaction was monitored by TLC, after finished, volatiles were removed under vacuum. Resulting residues were purified by C18Aq reverse phase column eluted with acetonitrile and water to achieve pure product **13a** (0.13 g, 50% yield). ^{1}H NMR (400 MHz, DMSO-d_6) δ 10.89 (s, 1H), 9.12 (s, 2H), 7.71 (d, J = 8.2 Hz, 2H), 7.61 (d, J = 16.0 Hz, 1H), 7.57 (d, J = 8.2 Hz, 2H), 7.41 (d, J = 7.7 Hz, 1H), 7.26 (d, J = 7.8 Hz, 1H), 7.04–6.98 (m, 1H), 6.97 – 6.91 (m, 1H), 6.71 (d, J = 15.9 Hz, 1H), 4.26 (s, 2H), 3.06 (s, 2H), 3.04–2.98 (m, 2H), 2.98–2.91 (m, 2H), 2.33 (s, 3H), 1.62–1.50 (m, 2H), 0.92 (t, J = 7.4 Hz, 3H). ^{13}C NMR (101 MHz, DMSO-d_6) δ 164.31, 140.56, 135.70, 135.44, 134.28, 133.16, 130.93, 128.56, 128.21, 120.72, 119.85, 118.82, 117.52, 111.07, 105.41, 52.52, 50.02, 47.48, 21.14, 19.27, 11.57, 11.53. HRMS (AP-ESI) m/z calcd for $C_{23}H_{29}N_5O$ [M + H]+ 391.24923, found 391.24972.

(*E*)-N-(4-(3-(2-(2-ammonioethyl)hydrazinyl)-3-oxoprop-1-en-1-yl)benzyl)-2-(2-methyl-1H-indol-3-yl)ethanaminium 2,2,2-trifluoroacetate (13b)—Using the synthetic method of **12a** and **13a**, **11** gave **13b** as a pale solid. ^{1}H NMR (400 MHz, DMSO-d_6) δ 10.90 (s, 1H), 9.76 (s, 1H), 9.08 (s, 2H), 7.82 (s, 3H), 7.67 (d, J = 8.2 Hz, 2H), 7.56 (d, J = 8.4 Hz, 2H), 7.52 (d, J = 15.9 Hz, 1H), 7.41 (d, J = 7.7 Hz, 1H), 7.26 (d, J = 7.8 Hz, 1H), 7.04–6.98 (m, 1H), 6.98–6.92 (m, 1H), 6.65 (d, J = 15.8 Hz, 1H), 4.25 (d, J = 5.4 Hz, 2H), 3.06–3.00 (m, 4H), 2.95 (t, J = 5.8 Hz, 2H), 2.86 (s, 2H), 2.33 (s, 3H). ^{13}C NMR (101 MHz, DMSO-d_6) δ 166.00, 139.26, 135.75, 134.04, 133.22, 131.00, 128.42, 128.26, 121.15, 120.79, 118.89, 117.59, 111.14, 105.49, 50.05, 48.53, 47.50, 37.37, 21.19, 11.62. ESI-MS m/z: 392.17 [M + H]+. HRMS (AP-ESI) m/z calcd for $C_{23}H_{29}N_5O$ [M + H]+ 392.24449, found 392.24384.

(*E*)-N-(4-(3-(2-(2-cyanoethyl)hydrazinyl)-3-oxoprop-1-en-1-yl)benzyl)-2-(2-methyl-1H-indol-3-yl)ethanaminium 2,2,2-trifluoroacetate (13c)—Compound **11** (0.45 g, 1 mmol) was dissolved in ethanol followed by the addition of Acrylonitrile (0.066 g, 1.25 mmol), the mixed solution was refluxed at 80 °C for 48 h. Volatiles were evaporated under vacuum, the crude product was purified by C18Aq column on reverse phase columns eluted with acetonitrile and water to achieve pure product **12c** (0.25 g, 50% yield). ESI-MS m/z: 446.17 [M + H]+. Using the synthetic method of **13a**, **12c** gave **13c** as a pale solid. ^{1}H NMR (400 MHz, DMSO-d_6) δ 10.89 (s, 1H), 9.76 (s, 1H), 9.00 (s, 2H), 7.66 (d, J = 8.2 Hz, 2H), 7.55 (d, J = 8.4 Hz, 2H), 7.51 (d, J = 15.9 Hz, 1H), 7.41 (d, J = 7.6 Hz, 1H), 7.26 (d, J = 7.8 Hz, 1H), 7.05–6.98 (m, 1H), 6.98–6.92 (m, 1H), 6.59 (d, J = 15.9 Hz, 1H), 4.25 (t, J = 5.5 Hz, 2H), 3.06 (s, 2H), 3.01–2.97 (m, 4H), 2.62 (t, J = 6.4 Hz, 2H), 2.33 (s, 3H). ^{13}C NMR (101 MHz, DMSO-d_6) δ 164.95, 138.81, 135.88, 135.75, 133.92, 133.22, 131.01, 128.33, 128.28, 121.38, 120.78, 120.41, 118.88, 117.62, 111.13, 105.52, 50.05, 47.51, 47.22, 21.17, 16.84, 11.62. ESI-MS m/z: 402.25 [M + H]+. HRMS (AP-ESI) m/z calcd for $C_{24}H_{27}N_5O$ [M + H]+ 402.22884, found 402.22818.

(*E*)-*N*-(4-(3-(2-(3-methoxy-3-oxopropyl)hydrazinyl)-3-oxoprop-1-en-1-yl)benzyl)-2-(2-methyl-1H-indol-3-yl)ethanaminium 2,2,2-trifluoroacetate (13d)
—Using the synthetic method of **12c**, compound **11** and methyl acrylate gave compound **12d**. ESI-MS m/z: 535.25 [M + H]+. Using the synthetic method of **13a**, **12d** gave **13d** as a

pale solid. ^{1}H NMR (400 MHz, DMSO-d_6) δ 10.91 (s, 1H), 10.02 (s, 1H), 9.15 (s, 2H), 7.66 (d, J = 8.2 Hz, 2H), 7.56 (d, J = 8.3 Hz, 2H), 7.52 (d, J = 15.8 Hz, 1H), 7.42 (d, J = 7.7 Hz, 1H), 7.26 (d, J = 7.8 Hz, 1H), 7.04–6.98 (m, 1H), 6.98–6.92 (m, 1H), 6.63 (d, J = 15.9 Hz, 1H), 4.25 (t, J = 5.3 Hz, 2H), 3.61 (s, 3H), 3.08–3.03 (m, 6H), 2.54–2.52 (m, 2H), 2.33 (s, 3H). ^{13}C NMR (101 MHz, DMSO-d_6) δ 172.54, 164.53, 139.12, 135.84, 135.75, 133.98, 133.23, 131.00, 128.41, 128.27, 121.03, 120.80, 118.89, 117.60, 111.14, 105.48, 51.94, 50.09, 47.53, 47.11, 32.43, 21.20, 11.63. ESI-MS m/z: 435.25 [M + H]$^+$. HRMS (AP-ESI) m/z calcd for C25H30N4O3 [M + H]+ 435.23907, found 435.23871

tert-butyl 4-(hydrazinecarbonyl)benzyl(2-(2-methyl-1H-indol-3-yl)ethyl)carbamate (14a)—Compound **6a** (0.42 g, 1 mmol) was dissolved in 20 mL methanol followed by the addition of 0.25 g (5 mmol) hydrazide monohydrate. The mixed solution was refluxed at 80 °C for 48 hours, after the reaction finished, volatiles were removed to afford product **14a** (0.34 g, 80% yield). ^{1}H NMR (400 MHz, DMSO-d_6) δ 10.71 (s, 1H), 9.72 (s, 1H), 7.79 (d, J = 8.2 Hz, 2H), 7.36–7.18 (m, 4H), 7.01–6.86 (m, 2H), 4.47 (d, J = 18.9 Hz, 2H), 3.29–3.19 (m, 2H), 2.82–2.72 (m, 2H), 2.27 (s, 3H), 1.36 (s, 9H). ESI-MS m/z: 423.17 [M + H]$^+$.

tert-butyl 3-(hydrazinecarbonyl)benzyl(2-(2-methyl-1H-indol-3-yl)ethyl)carbamate (14b)—Using the synthetic method of **14a**, **6c** and hydrazide monohydrate gave **14b**. ^{1}H NMR (400 MHz, DMSO-d_6) δ 10.71 (s, 1H), 9.77 (s, 1H), 7.78–7.64 (m, 2H), 7.47–7.26 (m, 3H), 7.21 (d, J = 7.9 Hz, 1H), 7.00–6.87 (m, 2H), 4.45 (s, 2H), 3.24 (s, 2H), 2.84–2.66 (m, 2H), 2.27 (s, 3H), 1.38 (s, 9H). ESI-MS m/z: 423.17 [M + H]$^+$.

tert-butyl benzyl(4-(hydrazinecarbonyl)benzyl)carbamate (14c)—Using the synthetic method of **14a**, **10a** and hydrazide monohydrate gave **14c**. ^{1}H NMR (400 MHz, DMSO-d_6) δ 9.74 (s, 1H), 7.79 (d, J = 8.3 Hz, 2H), 7.35 (t, J = 7.2 Hz, 2H), 7.31–7.20 (m, 5H), 4.55–4.29 (m, 6H), 1.39 (s, 9H). ESI-MS m/z: 356.17 [M + H]$^+$.

tert-butyl (2-(2-methyl-1H-indol-3-yl)ethyl)(4-(2-propylhydrazinecarbonyl)benzyl)carbamate (15a)—Using the synthetic method of **12a**, compound **14a** and propionaldehyde gave compound **15a**. ^{1}H NMR (400 MHz, DMSO-d_6) δ 10.72 (s, 1H), 9.98 (d, J = 6.0 Hz, 1H), 7.79 (d, J = 8.2 Hz, 2H), 7.30 (t, J = 7.5 Hz, 2H), 7.21 (d, J = 7.9 Hz, 1H), 6.96 (t, J = 7.3 Hz, 1H), 6.90 (t, J = 7.1 Hz, 1H), 5.08 (d, J = 6.0 Hz, 1H), 4.45 (s, 1H), 4.33 (s, 1H), 3.28–3.21(m, 2H), 2.78–2.73 (m, 4H), 2.27 (s, 3H), 1.51–1.41 (m, 2H), 1.36 (s, 9H), 0.90 (t, J = 7.4 Hz, 3H). ^{13}C NMR (101 MHz, DMSO-d_6) δ 165.50, 155.53, 142.52, 135.64, 132.52, 128.65, 127.75, 127.70, 127.36, 120.39, 118.52, 117.49, 110.83, 107.44, 79.24, 53.55, 49.58, 47.47, 28.41, 23.31, 21.30, 12.10, 11.50. ESI-MS m/z: 465.00 [M + H]$^+$. HRMS (AP-ESI) m/z calcd for C$_{27}$H$_{36}$N$_4$O$_3$ [M + H]+ 465.28602, found 465.28555.

tert-butyl (2-(2-methyl-1H-indol-3-yl)ethyl)(3-(2-propylhydrazinecarbonyl)benzyl)carbamate (15b)—Using the synthetic method of **12a**, compound **14b** and propionaldehyde gave compound **15b**. ^{1}H NMR (400 MHz, DMSO-d_6) δ 10.67 (s, 1H), 10.04 (s, 1H), 7.68 (d, J = 5.9 Hz, 2H), 7.43–7.33 (m, 3H), 7.21

(d, J = 7.9 Hz, 1H), 6.95 (t, J = 7.4 Hz, 1H), 6.88 (t, J = 6.8 Hz, 1H), 4.43 (s, 2H), 3.23 (s, 2H), 2.73 (t, J = 7.1 Hz, 4H), 2.25 (s, 3H), 1.49–1.40 (m, 2H), 1.35 (s, 9H), 0.89 (t, J = 7.4 Hz, 3H). ^{13}C NMR (101 MHz, DMSO-d_6) δ 165.77, 155.63, 135.58, 132.52, 128.60, 120.45, 118.58, 110.85, 107.45, 79.37, 53.50, 28.39, 21.21, 12.05, 11.42. HRMS (AP-ESI) m/z calcd for $C_{27}H_{36}N_4O_3$ [M + H]$^+$ 465.28602, found 465.28622.

tert-butyl benzyl(4-(2-propylhydrazinecarbonyl)benzyl)carbamate (15c)—Using the synthetic method of **12a**, compound **14c** and propionaldehyde gave compound **15c**. ^{1}H NMR (400 MHz, DMSO-d_6) δ 9.99 (s, 1H), 7.79 (d, J = 8.3 Hz, 2H), 7.37–7.34 (m, 2H), 7.31–7.20 (m, 5H), 5.10 (s, 1H), 4.38 (d, J = 21.7 Hz, 4H), 2.75 (t, J = 7.1 Hz, 2H), 1.50–1.42 (m, 2H), 1.39 (s, 9H), 0.91 (t, J = 7.4 Hz, 3H). ESI-MS *m/z*: 398.25 [M + H]$^+$. ^{13}C NMR (101 MHz, DMSO-d_6) δ 165.47, 155.53, 142.15, 138.62, 132.46, 128.95, 127.96, 127.68, 79.84, 53.55, 31.16, 28.43, 21.31, 12.14. HRMS (AP-ESI) m/z calcd for $C_{23}H_{31}N_3O_3$ [M + H]$^+$ 398.24382, found 398.24393.

2-(2-methyl-1H-indol-3-yl)-N-(4-(2-propylhydrazinecarbonyl)benzyl)ethanaminium 2,2,2-trifluoroacetate (16a)—Using the synthetic method of **13a**, **15a** gave **16a** as a pale solid. ^{1}H NMR (400 MHz, DMSO-d_6) δ 10.89 (s, 1H), 10.12 (s, 1H), 9.01 (s, 2H), 7.89 (d, J = 8.3 Hz, 2H), 7.59 (d, J = 8.3 Hz, 2H), 7.41 (d, J = 7.6 Hz, 1H), 7.26 (d, J = 7.7 Hz, 1H), 7.04–6.99 (m, 1H), 6.96 (td, J = 7.5, 1.1 Hz, 1H), 5.24 (s, 1H), 4.28 (s, 2H), 3.15–2.95 (m, 4H), 2.77 (t, J = 7.1 Hz, 2H), 2.33 (s, 3H), 1.56–1.40 (m, 2H), 0.92 (t, J = 7.4 Hz, 3H). ^{13}C NMR (101 MHz, DMSO-d_6) δ 165.14, 159.16, 158.85, 135.67, 133.98, 133.14, 130.22, 128.19, 127.84, 120.70, 119.15, 118.80, 117.51, 116.17, 111.05, 105.41, 53.45, 49.90, 47.51, 21.22, 21.11, 12.10, 11.53. HRMS (AP-ESI) m/z calcd for $C_{22}H_{28}N_4O$ [M + H]$^+$ 365.23359, found 365.23303.

2-(2-methyl-1H-indol-3-yl)-N-(3-(2-propylhydrazinecarbonyl)benzyl)ethanaminium 2,2,2-trifluoroacetate (16b)—Using the synthetic method of **13a**, **15b** gave **16b** as a pale solid. ^{1}H NMR (400 MHz, DMSO-d_6) δ 10.86 (s, 1H), 10.21 (s, 1H), 8.97 (s, 2H), 7.98 (s, 1H), 7.88–7.78 (m, 1H), 7.62 (d, J = 7.7 Hz, 1H), 7.51 (t, J = 7.7 Hz, 1H), 7.38 (d, J = 7.6 Hz, 1H), 7.21 (d, J = 7.8 Hz, 1H), 7.02–6.83 (m, 2H), 4.24 (s, 2H), 3.09–2.88 (m, 4H), 2.76 (t, J = 7.2 Hz, 2H), 2.29 (s, 3H), 1.51–1.36 (m, 2H), 0.88 (t, J = 7.4 Hz, 3H). ^{13}C NMR (101 MHz, DMSO-d_6) δ 165.41, 135.75, 133.99, 133.36, 133.22, 133.04, 129.82, 129.32, 128.27, 127.74, 120.81, 118.90, 117.60, 111.15, 105.46, 53.41, 50.25, 47.63, 21.21, 21.08, 12.13, 11.66. ESI-MS *m/z*: 365.17 [M + H]$^+$. HRMS (AP-ESI) m/z calcd for $C_{22}H_{28}N_4O$ [M + H]$^+$ 365.23359, found 363.23306.

N-benzyl-1-(4-(2-propylhydrazinecarbonyl)phenyl)methanaminium 2,2,2-trifluoroacetate (16c)—Using the synthetic method of **13a**, **15c** gave **16c** as a pale solid. ^{1}H NMR (400 MHz, DMSO-d_6) δ 9.98 (d, J = 3.9 Hz, 1H), 7.78 (d, J = 8.3 Hz, 2H), 7.42 (d, J = 8.3 Hz, 2H), 7.38–7.29 (m, 4H), 7.25–7.21 (m, 1H), 5.08 (d, J = 4.8 Hz, 1H), 3.72 (s, 2H), 3.67 (s, 2H), 2.75 (d, J = 2.7 Hz, 3H), 1.52–1.42 (m, 2H), 0.91 (t, J = 7.4 Hz, 3H). ^{13}C NMR (101 MHz, DMSO-d_6) δ 165.67, 144.78, 141.16, 131.94, 128.57, 128.38, 128.14,

127.38, 127.01, 53.58, 52.59, 52.22, 21.33, 12.15. HRMS (AP-ESI) m/z calcd for $C_{18}H_{23}N_3O$ [M + H]$^+$ 298.19139, found 298.19150.

methyl 4-benzamidobenzoate (19)—methyl 4-aminobenzoate (**18**, 0.30 g, 2 mmol) was dissolved in 20 mL DCM followed by the addition of benzoyl chloride (**17**, 0.28 g, 2 mmol) and TEA (0.4 mL, 3 mmol) at 0 °C, the mixture was allowed to react at room temperature overnight. After the reaction finished, organic solution was washed by saturated $NaHCO_3$ solution (2 × 30 mL), 1 M aqueous citric acid (2 × 30 mL), and brine (2 × 30 mL) and dried over $MgSO_4$ overnight. The solvent was evaporated, resulting residues were recrystallized by ethyl estate and hexane to yield **19**, a white solid (0.41 g, 80% yield). ^{1}H NMR (400 MHz, DMSO-d_6) δ 10.62 (s, 1H), 7.99–7.93 (m, 6H), 7.65–7.47 (m, 3H), 3.85 (s, 3H).

methyl 4-(benzyloxy)benzoate (22)—Phenylmethanol (**20**, 0.22 g, 2 mmol), methyl 4-hydroxybenzoate (**21**, 0.33 g, 2.2 mmol) and triphenylphosphine (0.79 g, 3 mmol) were dissolved in 40 mL anhydrous THF, to this solution was added Diethylazodicarboxylate (DEAD, 0.52 g, 3 mmol) at 0 °C. The reaction solution was allowed to stir at room temperature for 2 hours and monitored via TLC. After the reaction finished, volatiles were removed under vacuum, the crude product was purified by flash chromatography with hexanes and ethyl acetate to get pure product **22** (0.22 g, 45% yield). ESI-MS m/z: 243.17 [M + H]$^+$.

4-(benzylamino)benzohydrazide (23a)—Using the synthetic method of **14a**, **9b** and hydrazide monohydrate gave **23a**. ^{1}H NMR (400 MHz, DMSO-d_6) δ 9.29 (s, 1H), 7.59 (d, J = 8.8 Hz, 1H), 7.37–7.31 (m, 4H), 7.26–7.22 (m, 1H), 6.80 (t, J = 6.0 Hz, 1H), 6.57 (d, J = 8.8 Hz, 2H), 4.36–4.30 (m, 4H).

N-(4-(hydrazinecarbonyl)phenyl)benzamide (23b)—Using the synthetic method of **14a**, **19** and hydrazide monohydrate gave **23b**. ^{1}H NMR (400 MHz, DMSO-d_6) δ 10.45 (s, 1H), 9.70 (s, 1H), 7.99–7.96 (m, 2H), 7.88–7.83 (m, 4H), 7.65–7.54 (m, 3H), 4.47 (s, 2H). ESI-MS m/z: 256.17 [M + H]$^+$.

4-(benzyloxy)benzohydrazide (23c)—Using the synthetic method of **14a**, **22** and hydrazide monohydrate gave **23c**. ESI-MS m/z: 243.17 [M + H]$^+$.

N-(4-(2-propylhydrazinecarbonyl)benzyl)benzenaminium 2,2,2-trifluoroacetate (24a)—Using the synthetic method of **12a**, **23a** gave **24a** as a pale solid. ^{1}H NMR (400 MHz, DMSO-d_6) δ 9.55 (s, 1H), 7.56–7.48 (m, 2H), 7.34–7.24 (m, 4H), 7.21–7.16 (m, 1H), 6.78 (t, J = 6.1 Hz, 1H), 6.55–6.48 (m, 2H), 4.28 (d, J = 6.0 Hz, 2H), 2.65 (t, J = 7.1 Hz, 2H), 1.44–1.35 (m, 2H), 0.85 (t, J = 7.4 Hz, 3H). ^{13}C NMR (101 MHz, DMSO-d_6) δ 166.11, 151.66, 140.25, 128.95, 128.88, 127.69, 127.28, 120.45, 111.68, 53.88, 46.48, 21.39, 12.24. HRMS (AP-ESI) m/z calcd for $C_{17}H_{21}N_3O$ [M + H]$^+$ 284.17574, found 284.17574.

N-(4-(2-propylhydrazinecarbonyl)phenyl)benzamide (24b)—Using the synthetic method of **12a**, compound **23b** and propionaldehyde gave compound **24b**. ^{1}H NMR (400 MHz, DMSO-d_6) δ 10.46 (s, 1H), 9.95 (s, 1H), 8.00–7.95 (m, 2H), 7.90–7.81 (m, 4H), 7.65–7.59 (m, 1H), 7.58–7.52 (m, 2H), 5.09 (s, 1H), 2.75 (t, J = 7.1 Hz, 2H), 1.48–1.36 (m, 2H),

0.92 (t, *J* = 7.4 Hz, 3H). ^{13}C NMR (101 MHz, DMSO-*d*6) δ 166.37, 165.40, 142.37, 135.24, 135.19, 132.34, 130.77, 128.99, 128.58, 128.29, 119.97, 53.69, 21.41, 12.23. HRMS (AP-ESI) m/z calcd for $C_{17}H_{19}N_3O_2$ [M + H]+ 298.15500, found 298.15427.

4-(benzyloxy)-N'-propylbenzohydrazide (24c)—Using the synthetic method of **12a**, compound **23c** and propionaldehyde gave compound **24c**. ^{1}H NMR (400 MHz, DMSO-*d*6) δ 9.88 (s, 1H), 7.84–7.75 (m, 2H), 7.49–7.44 (m, 2H), 7.43–7.38 (m, 2H), 7.37–7.32 (m, 1H), 7.10–7.03 (m, 2H), 5.20–5.12 (m, 2H), 5.04 (s, 1H), 2.73 (t, *J* = 7.0 Hz, 2H), 1.53–1.37 (m, 2H), 0.91 (t, *J* = 7.4 Hz, 3H). ^{13}C NMR (101 MHz, DMSO-*d*6) δ 165.31, 161.05, 137.15, 129.27, 128.92, 128.40, 128.22, 126.04, 114.82, 69.76, 53.64, 21.33, 12.15. HRMS (AP-ESI) m/z calcd for $C_{17}H_{20}N_2O_2$ [M + H]+ 285.15975, found 285.15966.

(E)-N-(4-(3-(2,2-dimethylhydrazinyl)-3-oxoprop-1-en-1-yl)benzyl)-2-(2-methyl-1H-indol-3-yl)ethanaminium 2,2,2-trifluoroacetate (26a)—Using the synthetic method of **11**, compound **6a** and 1,1-dimethylhydrazine gave compound **25a**. ESI-MS *m/z*: 477.33 [M + H]+. Using the synthetic method of **13a**, **25a** gave **26a** as a pale solid ^{1}H NMR (400 MHz, DMSO-*d*6) δ 10.91 (s, 1H), 9.14 (s, 2H), 7.73–7.62 (m, 2H), 7.56–7.52 (m, 2H), 7.48–7.41 (m, 2H), 7.35 (d, *J* = 16.1 Hz, 1H), 7.26 (d, *J* = 7.8 Hz, 1H), 7.04–6.98 (m, 1H), 6.98–6.92 (m, 1H), 6.58 (d, *J* = 15.8 Hz, 1H), 4.25 (s, 2H), 3.06–3.01 (m, 4H), 2.54 (s, 6H), 2.33 (s, 3H). ^{13}C NMR (101 MHz, DMSO-*d*6) δ 166.94, 162.74, 158.93, 138.50, 135.94, 135.67, 133.68, 133.14, 130.90, 128.57, 128.19, 122.32, 120.71, 119.26, 118.80, 117.51, 116.17, 111.05, 105.41, 50.02, 48.52, 47.46, 46.87, 21.13, 11.57. HRMS (AP-ESI) m/z calcd for $C_{23}H_{28}N_4O$ [M + H]+ 377.23359, found 377.23434.

(E)-2-(2-methyl-1H-indol-3-yl)-N-(4-(3-oxo-3-(pyrrolidin-1-ylamino)prop-1-en-1-yl)benzyl)ethanaminium 2,2,2-trifluoroacetate (26b)—Using the synthetic method of **11**, compound **6a** and pyrrolidin-1-amine gave compound **25b**. ESI-MS *m/z*: 503.33 [M + H]+. Using the synthetic method of **13a**, **25b** gave **26b** as a pale solid ^{1}H NMR (400 MHz, DMSO-*d*6) δ 10.90 (s, 1H), 9.06 (s, 2H), 7.75–7.61 (m, 2H), 7.58–7.51 (m, 2H), 7.47 (d, *J* = 15.8 Hz, 1H), 7.41 (d, *J* = 7.5 Hz, 1H), 7.36 (d, *J* = 16.1 Hz, 1H), 7.26 (d, *J* = 7.8 Hz, 1H), 7.04–6.98 (m, 1H), 6.98–6.93 (m, 1H), 6.60 (d, *J* = 15.8 Hz, 1H), 4.24 (s, 2H), 3.06–3.00 (m, 4H), 2.88 (s, 4H), 2.33 (s, 3H), 1.72–1.82 (m, 4H). ^{13}C NMR (101 MHz, DMSO-*d*6) δ 167.50, 163.29, 159.01, 138.62, 136.15, 135.93, 135.67, 133.78, 133.72, 133.14, 130.90, 130.83, 128.21, 128.19, 122.08, 120.71, 118.81, 117.51, 111.05, 105.40, 55.89, 54.61, 50.03, 47.47, 22.33, 21.13, 11.56. HRMS (AP-ESI) m/z calcd for $C_{25}H_{30}N_4O$ [M + H]+ 403.24924, found 403.24993.

(E)-2-(2-methyl-1H-indol-3-yl)-N-(4-(3-oxo-3-(piperidin-1-ylamino)prop-1-en-1-yl)benzyl)ethanaminium 2,2,2-trifluoroacetate (26c)—Using the synthetic method of **11**, compound **6a** and piperidin-1-amine gave compound **25c**. ESI-MS *m/z*: 517.42 [M + H]+. Using the synthetic method of **13a**, **25c** gave **26c** as a pale solid ^{1}H NMR (400 MHz, DMSO-*d*6) δ 10.91 (s, 1H), 9.14 (s, 2H), 7.72–7.64 (m, 2H), 7.59–7.53 (m, 2H), 7.49 (d, *J* = 15.8 Hz, 1H), 7.42 (d, *J* = 7.7 Hz, 1H), 7.36 (d, *J* = 16.1 Hz, 1H), 7.26 (d, *J* = 7.8 Hz, 1H), 7.05–6.98 (m, 1H), 6.98–6.92 (m, 1H), 6.64 (d, *J* = 15.8 Hz, 1H), 4.31–4.17 (m, 2H), 3.06–2.98 (m, 4H), 2.89–2.76 (m, 4H), 2.32 (s, 3H), 1.70–1.51 (m, 4H), 1.39 (s, 2H). ^{13}C NMR

(126 MHz, DMSO-d_6) δ 162.62, 139.20, 135.83, 135.69, 133.82, 133.15, 130.90, 128.30, 128.19, 121.80, 120.73, 118.81, 117.51, 111.06, 105.37, 57.52, 50.06, 47.49, 24.94, 23.04, 21.15, 11.58. HRMS (AP-ESI) m/z calcd for $C_{26}H_{32}N_4O$ [M + H]$^+$ 417.26489, found 417.26410.

(E)-tert-butyl 4-(3-(2-ethyl-2-propylhydrazinyl)-3-oxoprop-1-en-1-yl)benzyl(2-(2-methyl-1H-indol-3-yl)ethyl)carbamate (27a)—**12a** (0.24 g, 0.5 mmol) was dissolved in methanol, then acetaldehyde (0.044 g, 1 mmol) was added, 2 hours later, NaBH$_3$CN (0.31 g, 5 mmol) was added followed by 2 drop of acetic acid. The mixed solution was allowed to stir overnight, after the reaction finished, volatiles were removed under vacuum. Resulting residues were purified by C18Aq reverse phase column eluted with acetonitrile and water to achieve pure product **27a** (0.12 g, 45% yield). ^{1}H NMR (400 MHz, DMSO-d_6) δ 10.71 (s, 1H), 7.55–7.50 (m, 2H), 7.40 (d, J = 15.8 Hz, 1H), 7.34–7.18 (m, 4H), 7.00–6.85 (m, 2H), 6.56 (d, J = 15.8 Hz, 1H), 4.36 (s, 2H), 3.23 (s, 2H), 2.84–2.71 (m, 4H), 2.70–2.60 (m, 2H), 2.27 (s, 3H), 1.44–1.40 (m, 2H), 1.37 (s, 9H), 0.97 (td, J = 7.1, 3.0 Hz, 3H), 0.86 (td, J = 7.4, 2.1 Hz, 3H). ESI-MS m/z: 519.33 [M + H]$^+$.

(E)-tert-butyl 4-(3-(2,2-dipropylhydrazinyl)-3-oxoprop-1-en-1-yl)benzyl(2-(2-methyl-1H-indol-3-yl)ethyl)carbamate (27b)—Using the synthetic method of **27a**, compounds **12a** and propanal gave **27b**. ESI-MS m/z: 533.42 [M + H]$^+$.

(E)-tert-butyl 4-(3-(2-butyl-2-propylhydrazinyl)-3-oxoprop-1-en-1-yl)benzyl(2-(2-methyl-1H-indol-3-yl)ethyl)carbamate (27c)—Using the synthetic method of **27a**, compounds **12a** and n-butanal gave **27c**. ESI-MS m/z: 547.42 [M + H]$^+$.

(E)-tert-butyl (2-(2-methyl-1H-indol-3-yl)ethyl)(4-(3-oxo-3-(2-pentyl-2-propylhydrazinyl)prop-1-en-1-yl)benzyl)carbamate (27d)—Using the synthetic method of **27a**, compounds **12a** and n-pentanal gave **27d**. ^{1}H NMR (400 MHz, DMSO-d_6) δ 10.70 (s, 1H), 8.16 (s, 1H), 7.61–7.48 (m, 2H), 7.39 (d, J = 15.7 Hz, 1H), 7.34–7.15 (m, 4H), 6.98–6,.89 (m, 2H), 6.54 (d, J = 15.8 Hz, 1H), 4.42 (s, 2H), 3.31–3.23 (m, 2H), 2.77 (s, 2H), 2.72–2.53 (m, 4H), 2.27 (s, 3H), 1.42–1.33 (m, 13H), 1.31–1.18 (m, 4H), 0.90–0.75 (m, 6H). ESI-MS m/z: 561.42 [M + H]$^+$.

(E)-tert-butyl 4-(3-(2-hexyl-2-propylhydrazinyl)-3-oxoprop-1-en-1-yl)benzyl(2-(2-methyl-1H-indol-3-yl)ethyl)carbamate (27e)—Using the synthetic method of **27a**, compounds **12a** and n-hexanal gave **27e**. ESI-MS m/z: 575.42 [M + H]$^+$.

(E)-N-(4-(3-(2-ethyl-2-propylhydrazinyl)-3-oxoprop-1-en-1-yl)benzyl)-2-(2-methyl-1H-indol-3-yl)ethanaminium 2,2,2-trifluoroacetate (28a)—Using the synthetic method of **13a**, compound **27a** gave **28a** as a pale solid ^{1}H NMR (400 MHz, DMSO-d_6) δ 10.88 (s, 1H), 9.11 (s, 2H), 7.67 (d, J = 7.3 Hz, 2H), 7.60–7.48 (m, 3H), 7.42–7.33 (m, 2H), 7.26 (d, J = 7.7 Hz, 1H), 7.00 (t, J = 7.2 Hz, 1H), 6.99–6.94 (m, 1H), 6.68 (d, J = 15.8 Hz, 1H), 4.23 (s, 2H), 3.05–2.95 (m, 6H), 2.90–2.78 (m, 2H), 2.32 (s, 3H), 1.49–1.38 (m, 2H), 1.01 (dt, J = 26.6, 6.7 Hz, 3H), 0.87 (t, J = 6.7 Hz, 3H). ^{13}C NMR (101 MHz, DMSO-d_6) δ 168.61, 164.29, 158.81, 136.16, 135.64, 133.97, 133.19, 130.91, 128.46, 128.15, 120.76, 118.86, 117.50, 111.07, 105.34, 60.21, 59.09, 50.06, 47.49, 21.09,

19.31,12.50, 12.09, 11.51. HRMS (AP-ESI) m/z calcd for $C_{26}H_{34}N_4O$ [M + H]$^+$ 419.28053, found 419.28153.

(E)-N-(4-(3-(2,2-dipropylhydrazinyl)-3-oxoprop-1-en-1-yl)benzyl)-2-(2-methyl-1H-indol-3-yl)ethanaminium 2,2,2-trifluoroacetate (28b)—Using the synthetic method of **13a**, compound **27b** gave **28b** as a pale solid ^{1}H NMR (400 MHz, DMSO-d_6) δ 10.91 (s, 1H), 9.12 (s, 2H), 7.66 (t, J = 8.3 Hz, 2H), 7.55 (d, J = 8.3 Hz, 2H), 7.48 (d, J = 16.1 Hz, 1H), 7.43–7.40 (m, 1H), 7.36 (d, J = 16.1 Hz, 1H), 7.26 (d, J = 7.8 Hz, 1H), 7.01 (t, J = 7.5 Hz, 1H), 6.98–6.91 (m, 1H), 6.66 (d, J = 15.8 Hz, 1H), 4.25 (t, J = 5.4 Hz, 2H), 3.13–2.92 (m, 4H), 2.76 (t, J = 7.2 Hz, 2H), 2.71–2.55 (m, 2H), 2.33 (s, 3H), 1.46–1.39 (m, 4H), 0.96–0.82 (m, 6H). ^{13}C NMR (101 MHz, DMSO-d_6) δ 168.25, 164.11, 159.19, 139.91, 136.20, 135.81, 135.68, 133.85, 133.14, 130.96, 128.29, 128.19, 120.69, 119.84, 118.80, 117.52, 111.05, 105.42, 60.62, 59.35, 50.01, 47.46, 21.12, 20.24, 19.92, 12.12, 11.90, 11.54. HRMS (AP-ESI) m/z calcd for $C_{27}H_{36}N_4O$ [M + H]$^+$ 433.29619, found 433.29717.

(E)-N-(4-(3-(2-butyl-2-propylhydrazinyl)-3-oxoprop-1-en-1-yl)benzyl)-2-(2-methyl-1H-indol-3-yl)ethanaminium 2,2,2-trifluoroacetate (28c)—Using the synthetic method of **13a**, compound **27c** gave **28c** as a pale solid ^{1}H NMR (400 MHz, DMSO-d_6) δ 10.91 (s, 1H), 9.15 (s, 2H), 7.67–7.64 (m, 2H), 7.56 (d, J = 8.4 Hz, 2H), 7.49 (d, J = 14.5 Hz, 1H), 7.41 (dd, J = 7.5, 3.7 Hz, 1H), 7.34 (d, J = 16.1 Hz, 1H), 7.26 (d, J = 7.9 Hz, 1H), 7.01 (t, J = 7.5 Hz, 1H), 6.98–6.91 (m, 1H), 6.67 (d, J = 15.8 Hz, 1H), 4.25 (t, J = 5.2 Hz, 2H), 3.15–2.92 (m, 4H), 2.82–2.75 (m, 2H), 2.73–2.55 (m, 2H), 2.33 (s, 3H), 1.50–1.24 (m, 6H), 0.93–0.77 (m, 6H). ^{13}C NMR (101 MHz, DMSO-d_6) δ 168.24, 164.05, 158.68, 136.20, 135.85, 135.67, 133.78, 133.14, 130.96, 130.89, 128.30, 128.27, 128.19, 120.70, 118.80, 118.58, 117.51, 111.05, 105.40, 60.61, 59.30, 50.01, 47.43, 29.12, 21.13, 20.24, 20.15, 14.35, 12.13, 11.56. HRMS (AP-ESI) m/z calcd for $C_{28}H_{38}N_4O$ [M + H]$^+$ 447.31183, found 447.31278.

(E)-2-(2-methyl-1H-indol-3-yl)-N-(4-(3-oxo-3-(2-pentyl-2-propylhydrazinyl)prop-1-en-1-yl)benzyl)ethanaminium 2,2,2-trifluoroacetate (28d)—Using the synthetic method of **13a**, compound **27d** gave **28d** as a pale solid ^{1}H NMR (400 MHz, DMSO-d_6) δ 10.89 (s, 1H), 8.99 (s, 2H), 7.68–7.63 (m, 2H), 7.58–7.52 (m, 2H), 7.52–7.38 (m, 2H), 7.35 (d, J = 16.1 Hz, 1H), 7.26 (d, J = 7.9 Hz, 1H), 7.01 (t, J = 7.5 Hz, 1H), 6.98–6.92 (m, 1H), 6.63 (d, J = 15.8 Hz, 1H), 4.24 (d, J = 5.1 Hz, 2H), 3.04 (d, J = 16.6 Hz, 4H), 2.78–2.53 (m, 4H), 2.33 (s, 3H), 1.45–1.23 (m, 8H), 0.90–0.77 (m, 6H). ^{13}C NMR (101 MHz, DMSO-d_6) δ 168.32, 164.12, 159.03, 139.92, 136.29, 136.00, 135.75, 133.87, 133.80, 133.23, 131.03, 130.98, 128.38, 128.33, 128.26, 120.80, 118.89, 117.60, 111.14, 105.47, 60.73, 59.29, 50.08, 47.53, 29.64, 26.71, 26.63, 22.59, 22.55, 21.21, 20.33, 20.28, 14.49, 12.21, 11.65. HRMS (AP-ESI) m/z calcd for $C_{29}H_{40}N_4O$ [M + H]$^+$ 461.32749, found 461.32721.

(E)-N-(4-(3-(2-hexyl-2-propylhydrazinyl)-3-oxoprop-1-en-1-yl)benzyl)-2-(2-methyl-1H-indol-3-yl)ethanaminium 2,2,2-trifluoroacetate (28e)—Using the synthetic method of **13a**, compound **27e** gave **28e** as a pale solid. ^{1}H NMR (400 MHz,

DMSO-d_6) δ 10.89 (s, 1H), 9.00 (s, 2H), 7.67–7.63 (m, 2H), 7.59–7.52 (m, 2H), 7.48 (d, $J =$ 13.8 Hz, 1H), 7.43–7.39 (m, 1H), 7.34 (d, $J =$ 16.1 Hz, 1H), 7.26 (d, $J =$ 8.0 Hz, 1H), 7.04–6.98 (m, 1H), 6.98–6.91 (m, 1H), 6.63 (d, $J =$ 15.8 Hz, 1H), 4.25 (s, 2H), 3.05–3.02 (m, 4H), 2.74–2.53 (m, 4H), 2.33 (s, 3H), 1.44–1.35 (m, 4H), 1.32–1.19 (m, 6H), 0.92–0.74 (m, 6H). ^{13}C NMR (101 MHz, DMSO-d_6) δ 168.33, 164.14, 158.95, 139.14, 136.29, 135.90, 135.75, 133.86, 133.22, 131.00, 128.38, 128.26, 120.79, 118.88, 117.59, 111.14, 105.47, 60.74, 59.39, 50.08, 47.54, 47.47, 31.67, 27.06, 26.99, 26.65, 22.59, 21.20, 20.32, 20.00, 14.38, 12.21, 11.99, 11.64. HRMS (AP-ESI) m/z calcd for $C_{30}H_{42}N_4O$ [M + H]$^+$ 475.34314, found 475.34277.

(E)-tert-butyl 4-(3-(2,2-bis(3-hydroxypropyl)hydrazinyl)-3-oxoprop-1-en-1-yl)benzyl(2-(2-methyl-1H-indol-3-yl)ethyl)carbamate (29)—Compound **11** (0.22 g, 0.5 mmol) was dissolved in 10mL ethanol, to this solution was added 3-Bromo-1-propanol (0.14 g, 1 mmol) followed by the addition of K_2CO_3 (0.27 g, 2 mmol). The mixture was refluxed at 90 °C for 1 hour, K_2CO_3 was filtered, the volatiles were removed under vacuum. Resulting residues were purified by C18Aq reverse phase column eluted with acetonitrile and water to achieve pure product **29** (0.20 g, 70% yield). ^{1}H NMR (400 MHz, MeOD) δ 8.34 (s, 1H), 7.67 (d, $J =$ 15.2 Hz, 1H), 7.42–7.21 (m, 4H), 7.15–6.99 (m, 4H), 6.36 (d, $J =$ 15.6 Hz, 1H), 4.31–4.16 (m, 2H), 3.74–3.62 (m, 4H), 3.36–3.27 (m, 2H), 2.91–2.60 (m, 6H), 2.24 (s, 3H), 1.71–1.63 (m, 4H), 1.47 (s, 9H). ESI-MS *m/z*: 565.42 [M + H]$^+$.

(E)-N-(4-(3-(2,2-bis(3-hydroxypropyl)hydrazinyl)-3-oxoprop-1-en-1-yl)benzyl)-2-(2-methyl-1H-indol-3-yl)ethanaminium 2,2,2-trifluoroacetate (30)—Using the synthetic method of **13a**, **29** gave **30** as a pale solid. ^{1}H NMR (400 MHz, DMSO-d_6) δ 10.90 (s, 1H), 9.15 (s, 2H), 7.69–7.63 (m, 2H), 7.56 (dd, $J =$ 8.3, 2.0 Hz, 2H), 7.52–7.38 (m, 2H), 7.33 (d, $J =$ 16.1 Hz, 1H), 7.26 (d, $J =$ 7.8 Hz, 1H), 7.00 (dd, $J =$ 11.0, 4.0 Hz, 1H), 6.95 (dd, $J =$ 10.7, 3.9 Hz, 1H), 6.65 (d, $J =$ 15.8 Hz, 1H), 4.25 (s, 2H), 3.49–3.44 (m, 4H), 3.08–3.00 (m, 4H), 2.86–2.56 (m, 4H), 2.33 (s, 3H), 1.64–1.47 (m, 4H). ^{13}C NMR (101 MHz, DMSO-D6) δ 164.38, 138.88, 135.96, 135.75, 133.21, 130.99, 128.46, 128.27, 120.77, 118.87, 117.61, 111.12, 105.53, 59.23, 55.01, 50.06, 49.13, 21.18, 11.59. HRMS (AP-ESI) m/z calcd for $C_{27}H_{36}N_4O_3$ [M + H]$^+$ 465.28602, found 465.28540.

Cell culture

All of the cell lines were purchased from ATCC. The MV4–11 cell line was cultured in Iscove's Modified Dulbecco's Medium (IMDM) supplemented with 10% fetal bovine serum (FBS) and 1% (v/v) Anti-Anti in 5% CO_2 at 37 °C. The HL-60 cell line was cultured in IMDM medium supplemented with 20% FBS and 1% (v/v) Anti-Anti in 5% CO_2 at 37 °C. Molm-14, RS4;11, and U937 were cultured in RPMI-1640 medium supplemented with 10% fetal bovine serum (FBS) and 1% (v/v) Anti-Anti in 5% CO_2 at 37 °C. Primary AML cells were cultured in RPMI-1640 medium supplemented with human hematopoietic stem cell expansion cytokine package (IL-3) from Peprotech. All human studies were approved by the Yale University Human Investigation Committee.

In vitro HDACs inhibition fluorescence assay

All of the HDAC enzymes were purchased from BPS Bioscience. *In vitro* HDAC inhibition assays were conducted as previously described.[26] In brief, 20 μL of recombinant HDAC enzyme solution (HDAC1–9) was mixed with various concentrations of tested compound (20 μL). The mixture was incubated at 30 °C for 1 h (for the time-dependent assay, the mixture was incubated for 15 min, 30 min, 60 min and 90 min, respectively), then 10 μL fluorogenic substrate (Boc-Lys (acetyl)-AMC for HDAC1, 2, 3, and 6, Boc-Lys (triflouroacetyl)-AMC for HDAC 4, 5, 7, 8, and 9) was added to a final concentration of 50 μM. After incubation at 30 °C for 2 h, the catalysis was stopped by addition of 10 μL of developer containing 30 mg/mL trypsin and 6 μM trichostatin A (TSA). 30 mins later, fluorescence intensity was measured using a microplate reader at excitation and emission wavelengths of 360 and 460 nm, respectively. The inhibition ratios were calculated from the fluorescence intensity readings of tested wells relative to those of control wells, and the IC_{50} curves and values were determined by GraphPad Prism 6.0, using the "log(inhibitor) vs. normalized response-variable slope" function.

HDACs 1 and 3 kinetics study

All of the HDAC enzymes were bought from BPS Bioscience. 40 μL of recombinant human HDAC enzyme (HDAC1 and 3) solution was added in 96-well format to black U-bottom plates. 40 μL of **13a** in HDAC buffer was added to a final concentration of 15 nM, 10 nM, 6.67 nM, 2.44 nM, and 2.96 nM for HDAC1 and 3, 2 nM, 1.33 nM, 0.89 nM, 0.59 nM for HDAC3, respectively. The mixture was allowed to incubate for 2 h at 30 °C before the addition of 20 μL of fluorogenic substrate Boc-Lys(acetyl)-AMC serially diluted from 200 μM to 25 μM, 2 times dilution. Two hours later, 20 μL of 5 mg/mL trypsin and 1 μM TSA solution was added to quench the reaction. Fluorescence was read at 360 nm (ex.)/460 nm (em.) using a Tecan M200 Pro. V_{max} and K_m were determined using GraphPad Prism's Michaelis-Menten function. Corresponding Lineweaver-Burke double reciprocal plots were derived from these values and plotted accordingly.

Molecular Docking Against HDAC1 and HDAC3

Docking sites were defined using sitefinder, and simulations used a rigid receptor and triangle matcher mythology for ligand site placement with London dG scoring. Thirty poses were calculated per binding site and the top 5 poses refined using GBVI/WSA rescoring (E_Score2, implemented in MOE 2019 from CCG). Structural files were PDB: 5ICN for HDAC1 and PDB: 4A69 for HDAC3.

MMP-2/MMP-9 inhibitory activity

The InnoZyme™ Gelatinase (MMP-2/MMP-9) Activity Assay Kit was purchased from EMD Chemicals, Inc. **13a** (45 μL), MMP inhibitor (positive control from Kit, 45 μL) and activation buffer (45 μL) were added to designated wells, the final comcentrations of **13a** were 50 μM and 10 μM. 45 μL of MMP-2/MMP-9 diluted in the activation buffer was then added to each well. After 10–15 min incubation, 10 μL substrate working solution was added. The mixture was incubated at 37 °C for 2 h, and fluorescence was read at 320 nm (ex.)/405 nm (em.) using a Tecan M200 Pro.

CD13 inhibition assay

40 μL of **13a** (final comcentrations were 50 μM and 10 μM) and CD13 inhibitor bestatin (final comcentrations was 10 μM) were added into 96-well clear plate followed by the addition of CD13 enzyme (microsomal aminopeptidase from porcine kidney microsomes, Sigma) solution. 5 min later, the substrate (*L*-leucine-p-nitroanilide) was added and the mixture was incubated at 37 °C for 30 min. The absorbance was measured at 405 nm with a microplate reader.

EC_{50} analysis.—MV4–11 (20,000 per well) or primary leukemia (100,000 per well) cells were plated in 96-well clear plates and pre-incubated overnight, then serially diluted inhibitors (3 times dilution) with 12 concentrations from 5 μM were added. Cells were incubated with compounds for 48 h. CellTiter-Blue was added to a final concentration of 0.125 mg/mL. The mixture was allowed to incubate for 2–4 h until sufficient color changed occurred. Cell viability was measured as a function of resorufin fluorescence intensity using a Tecan M200 Pro spectrophotometer, 560 nm/590 nm (excitation/emission). Data were normalized to control wells and background was removed. EC_{50}s were determined using GraphPad Prism's "log(inhibitor) vs. normalized response-variable slope" function.

NCI-60 screening methodology

All cell lines were maintained in RPMI1640 medium containing 10% FBS at 37°C in a 5% CO_2 humidified incubator. 5,000–10,000 cells were plated per well in 96-well clear plates and pre-incubated overnight. CellTiter-Blue was added to selected wells to a final concentration of 0.125 mg/mL to present a measurement of the cell population for each cell line at the time of drug addition (T_Z). At the same time, serially 10 times diluted inhibitor **13a** (6 concentrations) and medium at the same volume (100% control) was added to the rest wells, the maximal final concentration was 10 μM. Following drug addition, the plates were incubated for an additional 48 h at 37°C in a 5% CO_2, then CellTiter-Blue was added to each well to a final concentration of 0.125 mg/mL. The mixture was allowed to incubate for 2–4 h until sufficient color change occurred. Cell viability was measured as a function of resorufin fluorescence intensity using a Tecan M200 Pro spectrophotometer, 560 nm/590 nm (excitation/emission). The absorbance of time zero (Tz), 100% control with no drugs (C), and test growth in the presence of the drug at 6 concentration levels (Ti) were used for calculation of percentage growth inhibition.

$$[(\text{Ti}-\text{Tz})/(\text{C}-\text{Tz})] \times 100 \text{ for concentrations for which Ti} > / = \text{Tz}$$

$$[(\text{Ti}-\text{Tz})/\text{Tz}] \times 100 \text{ for concentrations for which Ti} < \text{Tz}$$

Dose-response parameters were calculated for each experimental agent. Growth inhibition of 50% (GI_{50}) was calculated from [(Ti-Tz)/(C-Tz)] ×100 = 50, which is the drug concentration resulting in a 50% reduction in control cells during the drug incubation. LC_{50} (concentration of drug resulting in a 50% reduction as compared to that at the beginning) was calculated from [(Ti-Tz)/Tz] ×100 = −50.

Western blot analysis

MV4–11 or HL-60 cells were plated (1,500,000 per well) in flat bottom 6-well plates and allowed to grow for 12 h, and then treated with desired drugs. Final concentrations of tested drugs were shown in the figure legends of Figure 3, Figure 5, Figure 6, Figure 7, and Figure 8. After treatment, cells were harvested, washed by PBS, and lysed with RIPA buffer, which was comprised of 50 mM Tris Base,150 mM NaCl, 5 mM EDTA, 0.1% (v/v) SDS, 0.5% (v/v) Sodium Deoxycholate, and 1% (v/v) Triton-x-100. After lysing, the suspension was ultra-sonicated and centrifuged at 14000 RPM for 15 min at 4°C. The mixture of 75 mL of supernatant and 25 mL of β-mercaptoethanol: NuPAGE® Lithium dodecyl sulfate (LDS) Sample Buffer (4X) (15:85) was heated at 90 °C for 15 min and normalized according to a BCA test before loading. Lysates were run on Invitrogen NuPAGE 4–12% Bis-Tris 15 well gels at 170 V for approximately 60 min in MES buffer. Gels were transferred to the methylcellulose membrane and ran at 30 V for 3 h. Membranes were incubated at 4 °C overnight with 1/1000 primary antibodies, which were diluted in 2.5% (w/v) milk or 5% (w/v) bovine serum albumin. The membrane was washed twice with Tris-buffered saline and with Tween (TBST buffer) before incubation with secondary antibodies. Images were acquired using a GE ImageQuant LAS 4000.

Antibodies

Ac-Histone H3 (Lys9/14)-R, Ac-Histone H4 (Ser 1/Lys 5/Lys 8/Lys 12), acetylated α-tubulin (6–11B-1), Flt-3/Flk-2 (C-20), STAT5 (A-9), p-ERK 1/2 (Thr202/Tyr204)-R, HSP70 (K-20), p53 (DO-1), XIAP (E-2), caspase-3 (31A1067), ERK 1 (K-23), p-p53 (59. Ser315), MDM2 (SMP14) and Flip$_{S/L}$ (G-11) antibodies were purchased from Santa Cruz Biotechnology. Actin and LC3B antibodies were purchased from Abcam.

Combination index (CI) test

20,000 MV4–11 cells were plated per well in 96-well clear plates and pre-incubated overnight, then serially diluted **13a** and RG7388, bortezomib, or 17-AAG were added alone and combined. For the experiment for **13a** and RG7388, concentration of **13a** was 25 nM, RG7388 was 2 times dilution from 500 nM. For the experiment of **13a** and bortezomib, concentrations of **13a** were 405 nM, 135 nM, 45 nM, 15 nM, and 5 nM, respectively, while concentration of bortezomib was 8 nM. In the experiment of **13a** in combination with 17-AAG, final comcentration of **13a** was 9.87 nM, concentrations of 17-AAG were 300 nM, 200 nM, 133 nM, 88 nM, and 59 nM, respectively. Then cells were incubated for 24 h (RG7388 and bortezomib) and 48 h (17-AAG), CellTiter-Blue was added to each well to a final concentration of 0.125 mg/mL. The mixture was allowed to incubate for 2–4 h until sufficient color changed occurred. Cell viability was measured as a function of resorufin fluorescence intensity using a Tecan M200 Pro spectrophotometer, 560 nm/590 nm (excitation/emission). The combination index (CI) was calculated using CompuSyn software.

MV4–11 cells rescue study

MV4–11 cells were maintained in IMDM medium containing 10% FBS at 37 °C in a 5% CO_2 humidified incubator. Cells were plated (50,000 per well) in flat-bottom 24-well plates

and allowed to grow for 12 h, then CellTiter-Blue was added to selected wells to a final concentration of 0.125 mg/mL to measure the cell viability at the time of inhibitor addition (t = 0), and was incubated for 2–4 h until sufficient color changed occurred. At the same time, the remaining wells were treated with **13a** (200 nM), **13a** (200 nM) with z-VAD (20 μM), chloroquine (5 μM) or wortmannin (100 nM) for 24 h. CellTiter-Blue was added to each well to a final concentration of 0.125 mg/mL. The mixture was allowed to incubate for the same time as the t = 0 wells. Cell viability was measured as a function of resorufin fluorescence intensity using a Tecan M200 Pro spectrophotometer, 560 nm/590 nm (excitation/emission). Data were normalized to control wells and background was removed. Cell viability with each treatment was compared with t = 0.

Mini-Ames tests

Compound mutagenic properties were tested using EBPI's Modified Ames ISO kit. Bacterial strains used in this test carry a specific mutation in the histidine biosynthesis pathway. As a result, Ames strains are histidine dependent and will not survive in histidine-deficient media. However, specific mutations caused by toxicant interactions at sites in the bacterial DNA can produce reversions back to the wild type genome, a state in which the bacteria regain the ability to synthesize histidine. Lyophilized *Salmonella typhimurium* strain (with modified TA100) was rehydrated in growth media, covered with a rubber stopper, and incubated at 37 °C with shaking for 16 h. Overnight TA100 cultures were diluted to OD_{600} = 0.05 into 1× Exposure media. To a 24 well plate, 1600 μL of water was added into negative control and sterility control wells while 1550 μL of water with 50 μL of 2-aminoanthracene (2-AA) was added into positive control wells. 1600 μL sterilized inhibitor solution was added into "No dilution" wells to a final concentration of 10 μM. Four sets of serial dilutions of compounds were performed in a separate sterilized container. 1.6 mL of diluted sample was transferred into the appropriate wells of the 24-well exposure plate. As 2-AA is a pro-mutagen that needs metabolic bioactivation through the use of S9 liver homogenate, 68 μL of S9 mix was added followed by the addition of 200 μL exposure solution containing D-glucose, D-biotin and bit of L-histidine. Then 200 μL of the overnight culture was added to all wells, except the sterility control well, and the mixture was allowed to incubate at 37 °C for 100 min. 1600 μL mixture was transferred from each well of the exposure plate to conical tubes and 8 mL reversion media was added. Each tube was vortex-mixed and emptied onto a loading boat. Using a multichannel pipette, 200 μL of the reversion mix from the reagent boats were immediately aliquoted into a 96 well plate (one 15 mL conical tube should be aliquoted in 48 wells from the 96 well plate). Plates were sealed into the included zip-top bags and the 96 well plates were incubated for 2–3 days at 37 °C (no shaking). Plates were scored visually; yellow and partial yellow wells are scored as positive while purple wells are scored as negative.

Pharmacokinetics study

All animal experiments were conducted under the guidelines of the "Guide for the care and use of laboratory animals" published by the National Institutes of Health (revised 2011) and under the approval of the Institutional Animal Care and Use Committee (IACUC# IACUC-2017–00079) of the Medical University of South Carolina (MUSC). Male CD-1 Mice (Charles River Laboratories) were fed a standard laboratory rodent diet and housed in

individual cages on a 12 h light and 12 h dark cycle with room temperature maintained at 22 $\pm$ 3 °C and relative humidity at 50 $\pm$ 20%. Animals were typically fasted overnight before dosing, with food returned after the 6 h blood samples were obtained. Compound **13a** was dissolved in PBS containing 5% DMSO. Intravenous bolus injection (iv) and oral gavage (po) were performed at a dose of 5 mg/kg and 20 mg/kg with a volume of 10 mL/kg, respectively. 3 mice were used for iv and po administration. All blood samples (100–300 μL per sample) were taken via appropriate vein (saphenous, jugular, or submandibular vein) at 5, 15, and 30 min and 1, 2, 4, 6, 8, and 24 h after dosing. Fluid replacement (1.5 mL of 0.9% sodium chloride injection, USP) was administered subcutaneously once after the 2 h blood sampling. Blood samples were collected in BD Microtainer tubes coated with anticoagulant, placed on ice, and within 30 min, centrifuged at $15,000 \times g$ for 5 min to obtain plasma samples. All plasma samples were stored at −70 °C until analysis.

Plasma samples were prepared as follows. Two or three volumes of acetonitrile containing internal standard were added to one volume of plasma to precipitate proteins. Samples were centrifuged ($3000 \times g$ for 10 min) and the supernatant removed for analysis by LC-MS/MS. Calibration standards and quality controls were made by preparation of a 1 mg/mL stock solution and subsequently a series of working solutions in methanol: water (1/:1, v/v) which were spiked into the blank plasma to yield a series of calibration standard samples in the range of 1 ng/mL to 10 μg/mL and quality control samples at three concentration levels (low, middle and high). All incurred PK/PD plasma samples were treated identically to the calibration standards and quality control samples. LC-MS-MS analysis was performed utilizing multiple reaction monitoring for detection of characteristic ions for each drug candidate, additional related analytes and internal standard.

Plasma concentrations were measured as described above to determine a concentration vs. time profile. The area under the plasma concentration vs. time curve (AUC) was calculated using the linear trapezoidal method. Fitting of the data to obtain pharmacokinetic parameters was carried out using non-compartmental analysis. Key PK parameters reported following intravenous administration are as follows: terminal half-life $t_{1/2}$, initial plasma concentration C_0, area under the plasma concentration vs. time curve AUC, the volume of distribution at steady-state V_{ss}, total plasma clearance CL_p, and mean residence time MRT. Key PK parameters reported following extravascular administration are as follows: terminal half-life $t_{1/2}$, maximum plasma concentration C_{max}, time to reach maximum plasma concentration t_{max}, area under the plasma concentration vs. time curve AUC, mean residence time MRT, and bioavailability F. All parameters are expressed for individual animals as well as mean, standard deviation, and coefficient of variation.

Supplementary Material

Refer to Web version on PubMed Central for supplementary material.

Acknowledgments

Abbreviations used

Ara-C	cytarabine
FLT3	FMS-like tyrosine kinase 3
IDH	isocitrate dehydrogenase
Bcl-2	B-cell lymphoma-2
NPM1	Nucleophosmin 1
STAT5	signal transducer and activator of transcription 5
XIAP	X-linked inhibitor of apoptosis
c-FLIP	cellular FLICE-like inhibitory protein
mTOR	mammalian target of rapamycin
DRAM	damage-regulated autophagy modulator
ZBG	zinc-binding group
HDACI	HDAC inhibitor
NaBH$_3$CN	sodium cyanoborohydride
Boc$_2$O	di-*tert*-butyl decarbonate
TEA	triethylamine
TBTU	*O*-(Benzotriazol-1-yl)-*N,N,N'*,*N'*-tetramethyluronium tetrafluoroborate
MgSO$_4$	magnesium sulfate anhydrous
PPh$_3$	triphenylphosphine
K$_2$CO$_3$	potassium carbonate
CS	catalytic site
AS	allosteric site
OS	overall survival
FLT3-ITD	FLT3 internal tandem duplication
GI$_{50}$	concentration for 50% of maximal inhibition of cell proliferation
LC$_{50}$	Median lethal concentration
C$_{max}$	mean peak plasma concentration

FL	FLT3 ligand
MDM2	murine double minute 2
CI	combination index

References

(1). Lowenberg B; Downing JR; Burnett A, Acute myeloid leukemia. N. Engl. J. Med 1999, 341, 1051–1062. [PubMed: 10502596]

(2). Redaelli A; Lee JM; Stephens JM; Pashos CL, Epidemiology and clinical burden of acute myeloid leukemia. Expert Rev. Anticancer Ther 2003, 3, 695–710. [PubMed: 14599092]

(3). Tallman MS; Wang ES; Altman JK; Appelbaum FR; Bhatt VR; Bixby D; Coutre SE; De Lima M; Fathi AT; Fiorella M, Acute Myeloid Leukemia, Version 3.2019, NCCN Clinical Practice Guidelines in Oncology. J. Natl. Compr. Cancer Network 2019, 17, 721–749.

(4). Wei AH; Tiong S, Midostaurin, enasidenib, CPX-351, gemtuzumab ozogamicin, and venetoclax bring new hope to AML. Blood. 2017, 130, 2469–2474. [PubMed: 29051180]

(5). Miller KD; Nogueira L; Mariotto AB; Rowland JH; Yabroff KR; Alfano CM; Jemal A; Kramer JL; Siegel RL, Cancer treatment and survivorship statistics, 2019. Ca-Cancer J. Clin 2019, 69, 363–385. [PubMed: 31184787]

(6). Deschler B; Lubbert M, Acute myeloid leukemia: epidemiology and etiology. Cancer. 2006, 107, 2099–2107. [PubMed: 17019734]

(7). Druker BJ, Translation of the Philadelphia chromosome into therapy for CML. Blood. 2008, 112, 4808–4817. [PubMed: 19064740]

(8). Kindler T; Lipka DB; Fischer T, FLT3 as a therapeutic target in AML: still challenging after all these years. Blood. 2010, 116, 5089–5102. [PubMed: 20705759]

(9). Stirewalt DL; Radich JP, The role of FLT3 in haematopoietic malignancies. Nat. Rev. Cancer 2003, 3, 650–665. [PubMed: 12951584]

(10). Kelly LM; Liu Q; Kutok JL; Williams IR; Boulton CL; Gilliland DG, FLT3 internal tandem duplication mutations associated with human acute myeloid leukemias induce myeloproliferative disease in a murine bone marrow transplant model. Blood. 2002, 99, 310–318. [PubMed: 11756186]

(11). Verhaak RG; Goudswaard CS; van Putten W; Bijl MA; Sanders MA; Hugens W; Uitterlinden AG; Erpelinck CA; Delwel R; Lowenberg B; Valk PJ, Mutations in nucleophosmin (NPM1) in acute myeloid leukemia (AML): association with other gene abnormalities and previously established gene expression signatures and their favorable prognostic significance. Blood. 2005, 106, 3747–3754. [PubMed: 16109776]

(12). Ikeda H; Kanakura Y; Tamaki T; Kuriu A; Kitayama H; Ishikawa J; Kanayama Y; Yonezawa T; Tarui S; Griffin JD, Expression and functional role of the proto-oncogene c-kit in acute myeloblastic leukemia cells. Blood. 1991, 78, 2962–2968. [PubMed: 1720040]

(13). Neubauer A; Dodge RK; George SL; Davey FR; Silver RT; Schiffer CA; Mayer RJ; Ball ED; Wurster-Hill D; Bloomfield CD; et al., Prognostic importance of mutations in the ras proto-oncogenes in de novo acute myeloid leukemia. Blood. 1994, 83, 1603–1611. [PubMed: 8123851]

(14). Radich JP; Kopecky KJ; Willman CL; Weick J; Head D; Appelbaum F; Collins SJ, N-ras mutations in adult de novo acute myelogenous leukemia: prevalence and clinical significance. Blood. 1990, 76, 801–807. [PubMed: 2200539]

(15). Coghlan DW; Morley AA; Matthews JP; Bishop JF, The incidence and prognostic significance of mutations in codon 13 of the N-ras gene in acute myeloid leukemia. Leukemia. 1994, 8, 1682–1687. [PubMed: 7934163]

(16). Min YH; Eom JI; Cheong JW; Maeng HO; Kim JY; Jeung HK; Lee ST; Lee MH; Hahn JS; Ko YW, Constitutive phosphorylation of Akt/PKB protein in acute myeloid leukemia: its significance as a prognostic variable. Leukemia. 2003, 17, 995–997. [PubMed: 12750723]

(17). Birkenkamp KU; Geugien M; Lemmink HH; Kruijer W; Vellenga E, Regulation of constitutive STAT5 phosphorylation in acute myeloid leukemia blasts. Leukemia. 2001, 15, 1923–1931. [PubMed: 11753614]

(18). Milella M; Kornblau SM; Estrov Z; Carter BZ; Lapillonne H; Harris D; Konopleva M; Zhao S; Estey E; Andreeff M, Therapeutic targeting of the MEK/MAPK signal transduction module in acute myeloid leukemia. J. Clin. Invest 2001, 108, 851–859. [PubMed: 11560954]

(19). Grandage VL; Gale RE; Linch DC; Khwaja A, PI3-kinase/Akt is constitutively active in primary acute myeloid leukaemia cells and regulates survival and chemoresistance via NF-kappaB, Mapkinase and p53 pathways. Leukemia. 2005, 19, 586–594. [PubMed: 15703783]

(20). Patel JP; Gonen M; Figueroa ME; Fernandez H; Sun Z; Racevskis J; Van Vlierberghe P; Dolgalev I; Thomas S; Aminova O; Huberman K; Cheng J; Viale A; Socci ND; Heguy A; Cherry A; Vance G; Higgins RR; Ketterling RP; Gallagher RE; Litzow M; van den Brink MR; Lazarus HM; Rowe JM; Luger S; Ferrando A; Paietta E; Tallman MS; Melnick A; Abdel-Wahab O; Levine RL, Prognostic relevance of integrated genetic profiling in acute myeloid leukemia. N. Engl. J. Med 2012, 366, 1079–1089. [PubMed: 22417203]

(21). Fredly H; Gjertsen BT; Bruserud Ø, Histone deacetylase inhibition in the treatment of acute myeloid leukemia: the effects of valproic acid on leukemic cells, and the clinical and experimental evidence for combining valproic acid with other antileukemic agents. Clin. epigenet 2013, 5, 12–25.

(22). Matthews GM; Mehdipour P; Cluse LA; Falkenberg KJ; Wang E; Roth M; Santoro F; Vidacs E; Stanley K; House CM, Functional-genetic dissection of HDAC dependencies in mouse lymphoid and myeloid malignancies. Blood. 2015, 126, 2392–2403. [PubMed: 26447190]

(23). Wada T; Kikuchi J; Nishimura N; Shimizu R; Kitamura T; Furukawa Y, Expression levels of histone deacetylases determine the cell fate of hematopoietic progenitors. J. Biol. Chem 2009, 284, 30673–30683. [PubMed: 19736310]

(24). Mehdipour P; Santoro F; Botrugno O; Romanenghi M; Pagliuca C; Matthews G; Johnstone R; Minucci S, HDAC3 activity is required for initiation of leukemogenesis in acute promyelocytic leukemia. Leukemia. 2017, 31, 995–997. [PubMed: 28074065]

(25). McClure JJ; Zhang C; Inks ES; Peterson YK; Li J; Chou CJ, Development of Allosteric Hydrazide-Containing Class I Histone Deacetylase Inhibitors for Use in Acute Myeloid Leukemia. J. Med. Chem 2016, 59, 9942–9959. [PubMed: 27754681]

(26). Li X; Peterson YK; Inks ES; Himes RA; Li J; Zhang Y; Kong X; Chou CJ, Class I HDAC inhibitors display different antitumor mechanism in leukemia and prostatic cancer cells depending on their p53 status. J. Med. Chem 2018, 61, 2589–2603. [PubMed: 29499113]

(27). Wang H; Zhou W; Zheng Z; Zhang P; Tu B; He Q; Zhu W-G, The HDAC inhibitor depsipeptide transactivates the p53/p21 pathway by inducing DNA damage. DNA repair. 2012, 11, 146–156. [PubMed: 22112863]

(28). Ishii S; Kurasawa Y; Wong J; Yu-Lee L. y., Histone deacetylase 3 localizes to the mitotic spindle and is required for kinetochore–microtubule attachment. Proc. Natl. Acad. Sci. U. S. A 2008, 105, 4179–4184. [PubMed: 18326024]

(29). Stevens F; Beamish H; Warrener R; Gabrielli B, Histone deacetylase inhibitors induce mitotic slippage. Oncogene. 2008, 27, 1345–1354. [PubMed: 17828304]

(30). Aron JL; Parthun MR; Marcucci G; Kitada S; Mone AP; Davis ME; Shen T; Murphy T; Wickham J; Kanakry C, Depsipeptide (FR901228) induces histone acetylation and inhibition of histone deacetylase in chronic lymphocytic leukemia cells concurrent with activation of caspase 8–mediated apoptosis and down-regulation of c-FLIP protein. Blood. 2003, 102, 652–658. [PubMed: 12649137]

(31). Mitsiades CS; Mitsiades NS; McMullan CJ; Poulaki V; Shringarpure R; Hideshima T; Akiyama M; Chauhan D; Munshi N; Gu X, Transcriptional signature of histone deacetylase inhibition in multiple myeloma: biological and clinical implications. Proc. Natl. Acad. Sci. U. S. A 2004, 101, 540–545. [PubMed: 14695887]

(32). Rosato RR; Almenara JA; Kolla SS; Maggio SC; Coe S; Giménez MS; Dent P; Grant S, Mechanism and functional role of XIAP and Mcl-1 down-regulation in flavopiridol/vorinostat antileukemic interactions. Mol. Cancer Ther 2007, 6, 692–702. [PubMed: 17308065]

(33). Chen S; Dai Y; Pei X-Y; Grant S, Bim upregulation by histone deacetylase inhibitors mediates interactions with the Bcl-2 antagonist ABT-737: evidence for distinct roles for Bcl-2, Bcl-xL, and Mcl-1. Mol. Cell. Biol 2009, 29, 6149–6169. [PubMed: 19805519]

(34). Xargay-Torrent S; López-Guerra M; Saborit-Villarroya I; Rosich L; Campo E; Roué G; Colomer D, Vorinostat-induced apoptosis in mantle cell lymphoma is mediated by acetylation of proapoptotic BH3-only gene promoters. Clin. Cancer Res 2011, 17, 3956–3968. [PubMed: 21652541]

(35). Lindemann R; Newbold A; Whitecross K; Cluse L; Frew A; Ellis L; Williams S; Wiegmans A; Dear A; Scott C, Analysis of the apoptotic and therapeutic activities of histone deacetylase inhibitors by using a mouse model of B cell lymphoma. Proc. Natl. Acad. Sci. U. S. A 2007, 104, 8071–8076. [PubMed: 17470784]

(36). Yi C; Ma M; Ran L; Zheng J; Tong J; Zhu J; Ma C; Sun Y; Zhang S; Feng W, Function and molecular mechanism of acetylation in autophagy regulation. Science. 2012, 336, 474–477. [PubMed: 22539722]

(37). Mrakovcic M; Kleinheinz J; Fröhlich LF, Histone deacetylase inhibitor-induced autophagy in tumor cells: implications for p53. Int. J. Mol. Sci. 2017, 18, 1883–1912.

(38). Grant S; Dai Y, Histone deacetylase inhibitors and rational combination therapies In Advances in cancer research, Elsevier: 2012; Vol. 116, pp 199–237. [PubMed: 23088872]

(39). Gu W; Roeder RG, Activation of p53 sequence-specific DNA binding by acetylation of the p53 C-terminal domain. Cell. 1997, 90, 595–606. [PubMed: 9288740]

(40). Vousden KH; Lane DP, p53 in health and disease. Nat. Rev. Mol. Cell Biol. 2007, 8, 275–283. [PubMed: 17380161]

(41). Fridman JS; Lowe SW, Control of apoptosis by p53. Oncogene. 2003, 22, 9030–9040. [PubMed: 14663481]

(42). Bucher N; Britten C, G2 checkpoint abrogation and checkpoint kinase-1 targeting in the treatment of cancer. Br. J. Cancer 2008, 98, 523–528. [PubMed: 18231106]

(43). Crighton D; Wilkinson S; O'Prey J; Syed N; Smith P; Harrison PR; Gasco M; Garrone O; Crook T; Ryan KM, DRAM, a p53-induced modulator of autophagy, is critical for apoptosis. Cell. 2006, 126, 121–134. [PubMed: 16839881]

(44). Duvic M; Vu J, Update on the treatment of cutaneous T-cell lymphoma (CTCL): Focus on vorinostat. Biol.: Targets Ther 2007, 1, 377–392.

(45). Bertino EM; Otterson GA, Romidepsin: a novel histone deacetylase inhibitor for cancer. Expert Opin. Invest. Drugs 2011, 20, 1151–1158.

(46). Rashidi A; Cashen AF, Belinostat for the treatment of relapsed or refractory peripheral T-cell lymphoma. Future Oncol. 2015, 11, 1659–1664. [PubMed: 26043217]

(47). Greig SL, Panobinostat: a review in relapsed or refractory multiple myeloma. Target oncol. 2016, 11, 107–114. [PubMed: 26826025]

(48). Traoré MD; Zwick V; Simões-Pires CA; Nurisso A; Issa M; Cuendet M; Maynadier M; Wein S; Vial H; Jamet H, Hydroxyl ketone-based histone deacetylase inhibitors to gain insight into class I HDAC selectivity versus that of HDAC6. ACS Omega. 2017, 2, 1550–1562. [PubMed: 30023639]

(49). Micelli C; Rastelli G, Histone deacetylases: structural determinants of inhibitor selectivity. Drug discovery today. 2015, 20, 718–735. [PubMed: 25687212]

(50). Son SI; Cao J; Zhu CL; Miller SP; Lin H, Activity-guided design of HDAC11-specific inhibitors. ACS Chem. Biol 2019, 14, 1393–1397. [PubMed: 31264832]

(51). Wang Y; Stowe RL; Pinello CE; Tian G; Madoux F; Li D; Zhao LY; Li JL; Wang Y; Wang Y; Ma H; Hodder P; Roush WR; Liao D, Identification of histone deacetylase inhibitors with benzoylhydrazide scaffold that selectively inhibit class I histone deacetylases. Chem. Biol 2015, 22, 273–284. [PubMed: 25699604]

(52). Koechlin BA; Schwartz MA; Oberhaensli WE, Metabolism of C14-iproniazid and C14-isocarboxazid in man. J. Pharmacol. Exp. Ther 1962, 138, 11–20. [PubMed: 14034092]

(53). Nelson SD; Mitchell JR; Snodgrass W; Timbrell JA, Hepatotoxicity and metabolism of iproniazid and isopropylhydrazine. J. Pharmacol. Exp. Ther 1978, 206, 574–585. [PubMed: 702322]

(54). Girling D, The hepatic toxicity of antituberculosis regimens containing isoniazid, rifampicin and pyrazinamide. Tubercle. 1977, 59, 13–32.

(55). Clive S; Woo MM; Nydam T; Kelly L; Squier M; Kagan M, Characterizing the disposition, metabolism, and excretion of an orally active pan-deacetylase inhibitor, panobinostat, via trace radiolabeled 14 C material in advanced cancer patients. Cancer Chemother. Pharmacol 2012, 70, 513–522. [PubMed: 22864948]

(56). McClure JJ; Li X; Chou CJ Advances and challenges of HDAC inhibitors in cancer therapeutics In Advances in cancer research, Elsevier: 2018; Vol. 138, pp 183–211. [PubMed: 29551127]

(57). Steele NL; Plumb JA; Vidal L; Tjørnelund J; Knoblauch P; Rasmussen A; Ooi CE; Buhl-Jensen P; Brown R; Evans TJ, A phase 1 pharmacokinetic and pharmacodynamic study of the histone deacetylase inhibitor belinostat in patients with advanced solid tumors. Clin. Cancer Res 2008, 14, 804–810. [PubMed: 18245542]

(58). Kelly WK; Richon VM; O'Connor O; Curley T; MacGregor-Curtelli B; Tong W; Klang M; Schwartz L; Richardson S; Rosa E, Phase I clinical trial of histone deacetylase inhibitor. Clin. Cancer Res 2003, 9, 3578–3588. [PubMed: 14506144]

(59). Giles F; Fischer T; Cortes J; Garcia-Manero G; Beck J; Ravandi F; Masson E; Rae P; Laird G; Sharma S, A phase I study of intravenous LBH589, a novel cinnamic hydroxamic acid analogue histone deacetylase inhibitor, in patients with refractory hematologic malignancies. Clin. Cancer Res 2006, 12, 4628–4635. [PubMed: 16899611]

(60). Peschel I; Podmirseg SR; Taschler M; Duyster J; Götze KS; Sill H; Nachbaur D; Jäkel H; Hengst L; Tirol ÖK, FLT3 and FLT3-ITD phosphorylate and inactivate the cyclin dependent kinase inhibitor p27Kip1 in acute myeloid leukemia. haematologica. 2017,102, 1378–1389. [PubMed: 28522571]

(61). Mali RS; Lasater EA; Doyle K; Malla R; Boghaert E; Souers A; Leverson JD; Sampath D, Abstract B052: FLT3-ITD activation mediates resistance to the BCL-2 selective antagonist, venetoclax, in FLT3-ITD mutant AML models. Mol. Cancer Ther 2018, 17, B052–B052.

(62). Ranganathan P; Yu X; Santhanam R; Hofstetter J; Walker A; Walsh K; Bhatnagar B; Klisovic R; Vasu S; Phelps MA, Decitabine priming enhances the anti-leukemic effects of exportin 1 (XPO1) selective inhibitor selinexor in acute myeloid leukemia. Blood. 2015,125, 2689–2692. [PubMed: 25716206]

(63). Bradner JE; West N; Grachan ML; Greenberg EF; Haggarty SJ; Warnow T; Mazitschek R, Chemical phylogenetics of histone deacetylases. Nat. Chem. Biol 2010, 6, 238–243. [PubMed: 20139990]

(64). Mohamed MFA; Youssif BGM; Shaykoon MSA; Abdelrahman MH; Elsadek BEM; Aboraia AS; Abuo-Rahma GEA, Utilization of tetrahydrobenzo[4,5]thieno[2,3-d]pyrimidinone as a cap moiety in design of novel histone deacetylase inhibitors. Bioorg. Chem 2019, 91, 103127. [PubMed: 31374527]

(65). Atadja P, Development of the pan-DAC inhibitor panobinostat (LBH589): successes and challenges. Cancer lett. 2009, 280, 233–241. [PubMed: 19344997]

(66). Malkin D; Nichols KE; Zelley K; Schiffman JD, Predisposition to pediatric and hematologic cancers: a moving target. Am Soc Clin Oncol Educ Book. 2014, 34, e44–55.

(67). Network CGAR, Genomic and epigenomic landscapes of adult de novo acute myeloid leukemia. N. Engl. J. Med 2013, 368, 2059–2074. [PubMed: 23634996]

(68). Assi R; Gur HD; Loghavi S; Konoplev SN; Konopleva M; Daver N; Tashakori M; Kadia T; Routbort M; Salem A, P53 protein overexpression in de novo acute myeloid leukemia patients with normal diploid karyotype correlates with FLT3 internal tandem duplication and worse relaps-free survival. Am. J. Hematol 2018, 93, 1376–1383. [PubMed: 30117185]

(69). Levis M; Small D, FLT3: ITDoes matter in leukemia. Leukemia. 2003, 17, 1738–1752. [PubMed: 12970773]

(70). Choudhary C; Schwäble J; Brandts C; Tickenbrock L; Sargin B; Kindler T; Fischer T; Berdel WE; Müller-Tidow C; Serve H, AML-associated Flt3 kinase domain mutations show signal transduction differences compared with Flt3 ITD mutations. Blood. 2005, 106, 265–273. [PubMed: 15769897]

(71). Mizuki M; Schwäble J; Steur C; Choudhary C; Agrawal S; Sargin B; Steffen B; Matsumura I; Kanakura Y; Böhmer FD, Suppression of myeloid transcription factors and induction of STAT response genes by AML-specific Flt3 mutations. Blood. 2003, 101, 3164–3173. [PubMed: 12468433]

(72). Grundler R; Miething C; Thiede C; Peschel C; Duyster J, FLT3-ITD and tyrosine kinase domain mutants induce 2 distinct phenotypes in a murine bone marrow transplantation model. Blood. 2005, 105, 4792–4799. [PubMed: 15718420]

(73). Drexler H, Expression of FLT3 receptor and response to FLT3 ligand by leukemic cells. Leukemia. 1996, 10, 588–599. [PubMed: 8618433]

(74). Piacibello W; Fubini L; Sanavio F; Brizzi MF; Severino A; Garetto L; Stacchini A; Pegoraro L; Aglietta M, Effects of human FLT3 ligand on myeloid leukemia cell growth: heterogeneity in response and synergy with other hematopoietic growth factors. Blood. 1995, 86, 4105–4114. [PubMed: 7492767]

(75). Stacchini A; Fubini L; Severino A; Sanavio F; Aglietta M; Piacibello W, Expression of type III receptor tyrosine kinases FLT3 and KIT and responses to their ligands by acute myeloid leukemia blasts. Leukemia. 1996, 10, 1584–1591. [PubMed: 8847893]

(76). Calò V; Migliavacca M; Bazan V; Macaluso M; Buscemi M; Gebbia N; Russo A, STAT proteins: from normal control of cellular events to tumorigenesis. J. Cell. Physiol 2003, 197, 157–168. [PubMed: 14502555]

(77). Takahashi S; Harigae H; Kaku M; Sasaki T; Licht JD, Flt3 mutation activates p21 WAF1/CIP1 gene expression through the action of STAT5. Biochem. Biophys. Res. Commun 2004, 316, 85–92. [PubMed: 15003515]

(78). Kim K-T; Baird K; Ahn J-Y; Meltzer P; Lilly M; Levis M; Small D, Pim-1 is up-regulated by constitutively activated FLT3 and plays a role in FLT3-mediated cell survival. Blood. 2005, 105, 1759–1767. [PubMed: 15498859]

(79). Gilliland DG; Griffin JD, The roles of FLT3 in hematopoiesis and leukemia. Blood. 2002, 100, 1532–1542. [PubMed: 12176867]

(80). Safa A, c-FLIP, a master anti-apoptotic regulator. Exp. Oncol 2012, 34, 176–184. [PubMed: 23070002]

(81). Riedl SJ; Renatus M; Schwarzenbacher R; Zhou Q; Sun C; Fesik SW; Liddington RC; Salvesen GS, Structural basis for the inhibition of caspase-3 by XIAP. Cell. 2001, 104, 791–800. [PubMed: 11257232]

(82). Scott FL; Denault JB; Riedl SJ; Shin H; Renatus M; Salvesen GS, XIAP inhibits caspase-3 and −7 using two binding sites: evolutionarily conserved mechanism of IAPs. EMBO J. 2005, 24, 645–655. [PubMed: 15650747]

(83). Shiozaki EN; Chai J; Rigotti DJ; Riedl SJ; Li P; Srinivasula SM; Alnemri ES; Fairman R; Shi Y, Mechanism of XIAP-mediated inhibition of caspase-9. Mol cell. 2003, 11, 519–527. [PubMed: 12620238]

(84). Tanida I; Minematsu-Ikeguchi N; Ueno T; Kominami E, Lysosomal turnover, but not a cellular level, of endogenous LC3 is a marker for autophagy. Autophagy. 2005, 1, 84–91. [PubMed: 16874052]

(85). Quentmeier H; Reinhardt J; Zaborski M; Drexler H, FLT3 mutations in acute myeloid leukemia cell lines. Leukemia. 2003, 17, 120–124. [PubMed: 12529668]

(86). Ma L; Sato F; Sato R; Matsubara T; Hirai K; Yamasaki M; Shin T; Shimada T; Nomura T; Mori K, Dual targeting of heat shock proteins 90 and 70 promotes cell death and enhances the anticancer effect of chemotherapeutic agents in bladder cancer. Oncol. Rep 2014, 31, 2482–2492. [PubMed: 24718854]

(87). Beere HM; Wolf BB; Cain K; Mosser DD; Mahboubi A; Kuwana T; Tailor P; Morimoto RI; Cohen GM; Green DR, Heat-shock protein 70 inhibits apoptosis by preventing recruitment of procaspase-9 to the Apaf-1 apoptosome. Nat. Cell Biol 2000, 2, 469–475. [PubMed: 10934466]

(88). Garrido C; Schmitt E; Candé C; Vahsen N; Parcellier A; Kroemer G, HSP27 and HSP70: potentially oncogenic apoptosis inhibitors. Cell cycle. 2003, 2, 578–583.

(89). Ravagnan L; Gurbuxani S; Susin SA; Maisse C; Daugas E; Zamzami N; Mak T; Jäättelä M; Penninger JM; Garrido C, Heat-shock protein 70 antagonizes apoptosis-inducing factor. Nat. Cell Biol 2001, 3, 839–843. [PubMed: 11533664]

(90). Schrader A; Crispatzu G; Oberbeck S; Mayer P; Pützer S; Jan J; Vasyutina E; Warner K; Weit N; Pflug N, Actionable perturbations of damage responses by TCL1/ATM and epigenetic lesions form the basis of T-PLL. Nat. Commun 2018, 9, 697–719. [PubMed: 29449575]

(91). Andersson E; Pützer S; Yadav B; Dufva O; Khan S; He L; Sellner L; Schrader A; Crispatzu G; Ole M, Discovery of novel drug sensitivities in T-PLL by high-throughput ex vivo drug testing and mutation profiling. Leukemia. 2018, 32, 774–787. [PubMed: 28804127]

(92). D'Arcy MS, Cell death: a review of the major forms of apoptosis, necrosis and autophagy. Cell Biol Int. 2019, 43, 582–592. [PubMed: 30958602]

(93). Yeo P; Xin L; Goh E; New LS; Zeng P; Wu X; Venkatesh P; Kantharaj E, Development and validation of high-performance liquid chromatography-tandem mass spectrometry assay for 6-(3-benzoyl-ureido)-hexanoic acid hydroxyamide, a novel HDAC inhibitor, in mouse plasma for pharmacokinetic studies. Biomed. Chromatogr. 2007, 21, 184–189. [PubMed: 17221921]
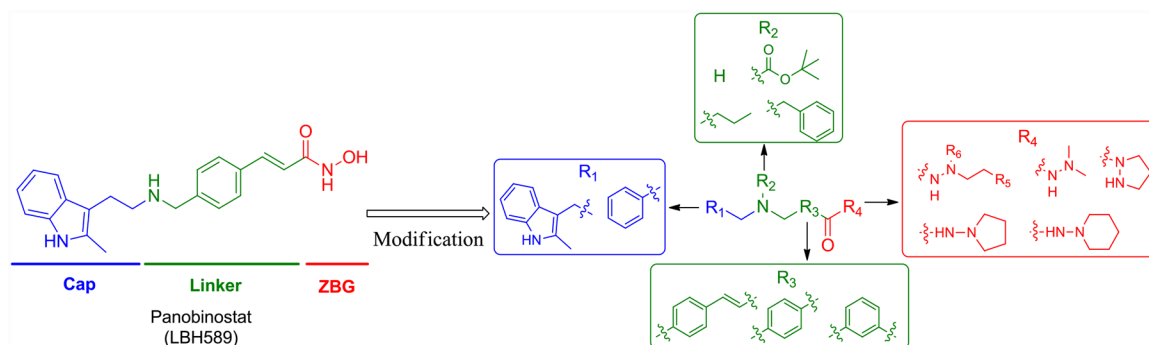
Figure 1.
Design of hydrazide-bearing HDACIs based on the structure of panobinostat.
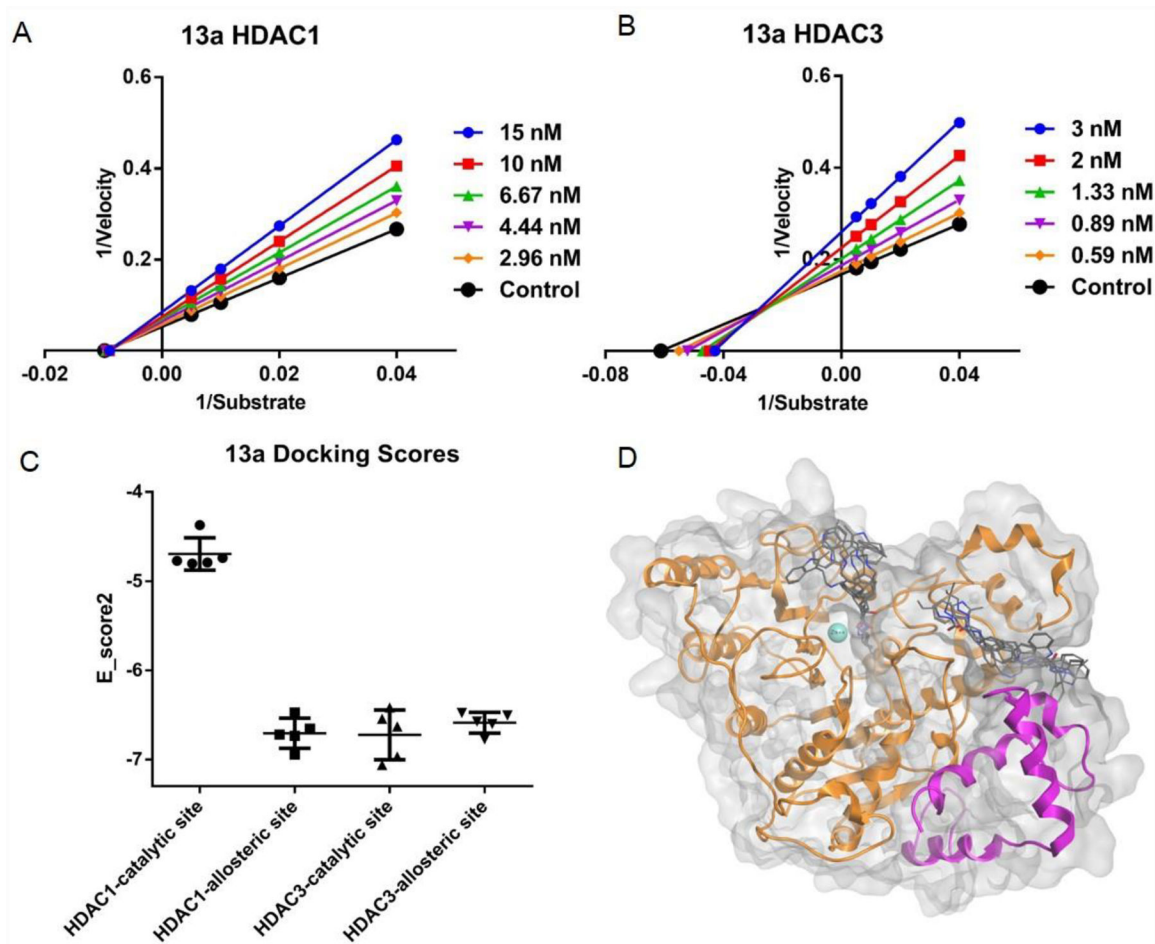
Figure 2A and B:

Lineweaver-Burke plots of enzyme kinetics data in the presence of inhibitors. Y-axes units: (pmoles acetylated substrate cleaved/min)$^{-1}$, Xaxes units: (µmoles)$^{-1}$. Compound **13a** for HDAC1, and 3, respectively. Intersection on Xaxes are indicative of non-competative inhibition (HDAC1, **3A**), while intersections in 2nd quadrant are indicative of mixed and competitive inhibition (HDAC3, **3B**). Representative plots of n ≥ 3 experiments. **2C**. Molecular docking probe of the catalytic and allosteric binding pockets of HDAC1 (PDB: 5ICN) and HDAC3 (PDB: 4A69). Data is represented as whisker plot using the top 5 docking poses for each condition. The catalytic site was defined as the catalytic pocket that incorporated the Zn metal iron, and the allosteric site was defined as the allosteric pocket created by the interface between the HDAC heterodimer. **2D**. Potential binding mode of **13a** with catalytic site and allosteric site of HDAC3 in silico. Top 5 docking poses for each site are displayed.
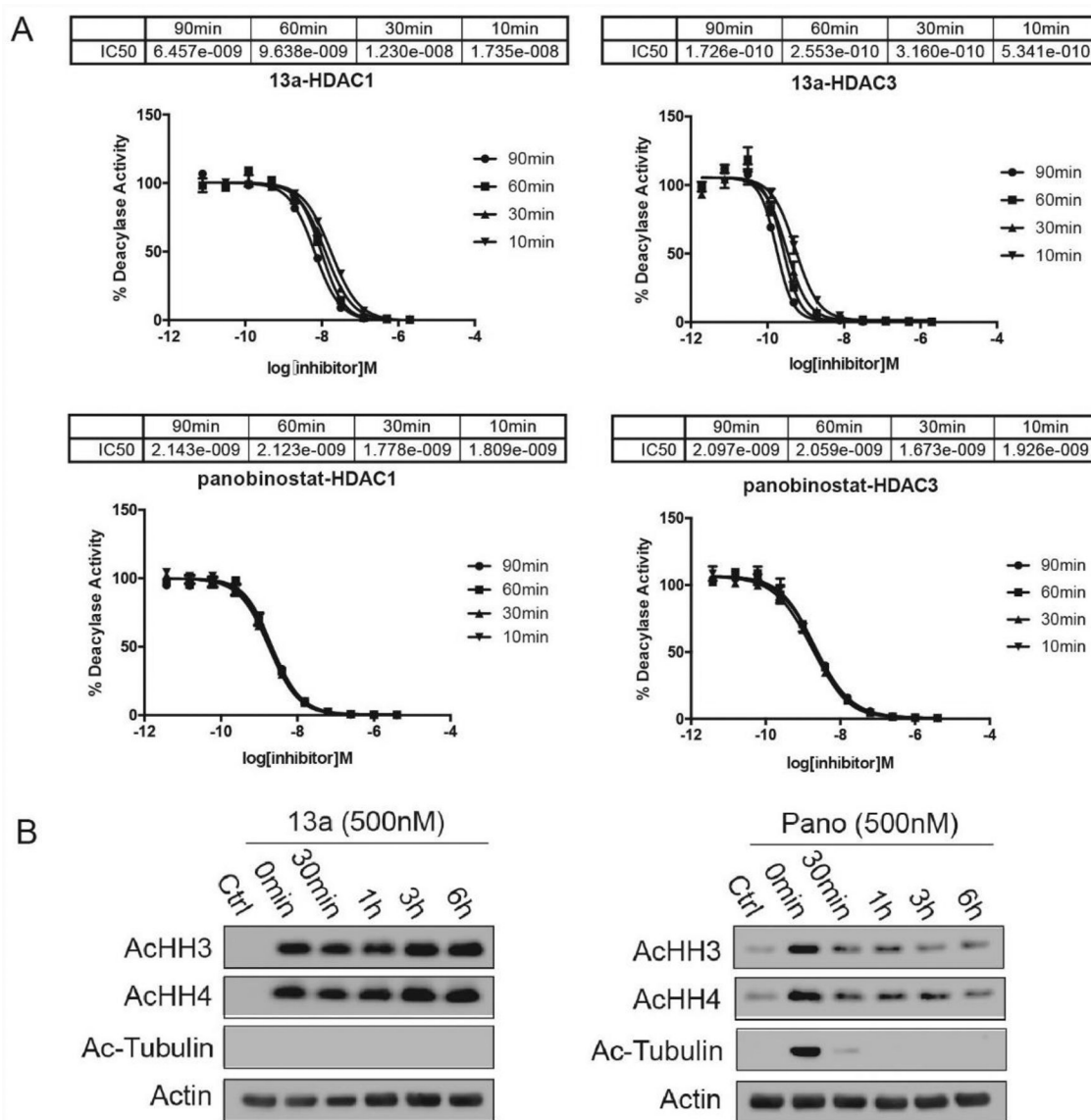
Figure 3A:

IC$_{50}$ curves of **13a** and panobinostat for HDACs 1, 2, and 3 after pre-incubation of 10 min, 30 min, 60 min, and 90 min, respectively. **13a** shows time-dependent inhibition toward HDAC1 and 3, which indicates slow-on inhibition; while panobinostat reaches a steady-state with 10 min pre-incubation, indicating fast-on kinetics. Dose response curves for **13a** and panobinostat performed in triplicates were generated using GraphPad Prism software. **3B**: Histone acetylation caused by **13a** does not reduce within 6 h of drug removal, while panobinostat reduces acetylation within 30 min after removal of drug. MV4–11 cells are treated with **13a** or panobinostat (Pano) for 3 h, control cells are collected for the 0 min point, the drugs are washed out and the cells are cultured for various lengths of time.
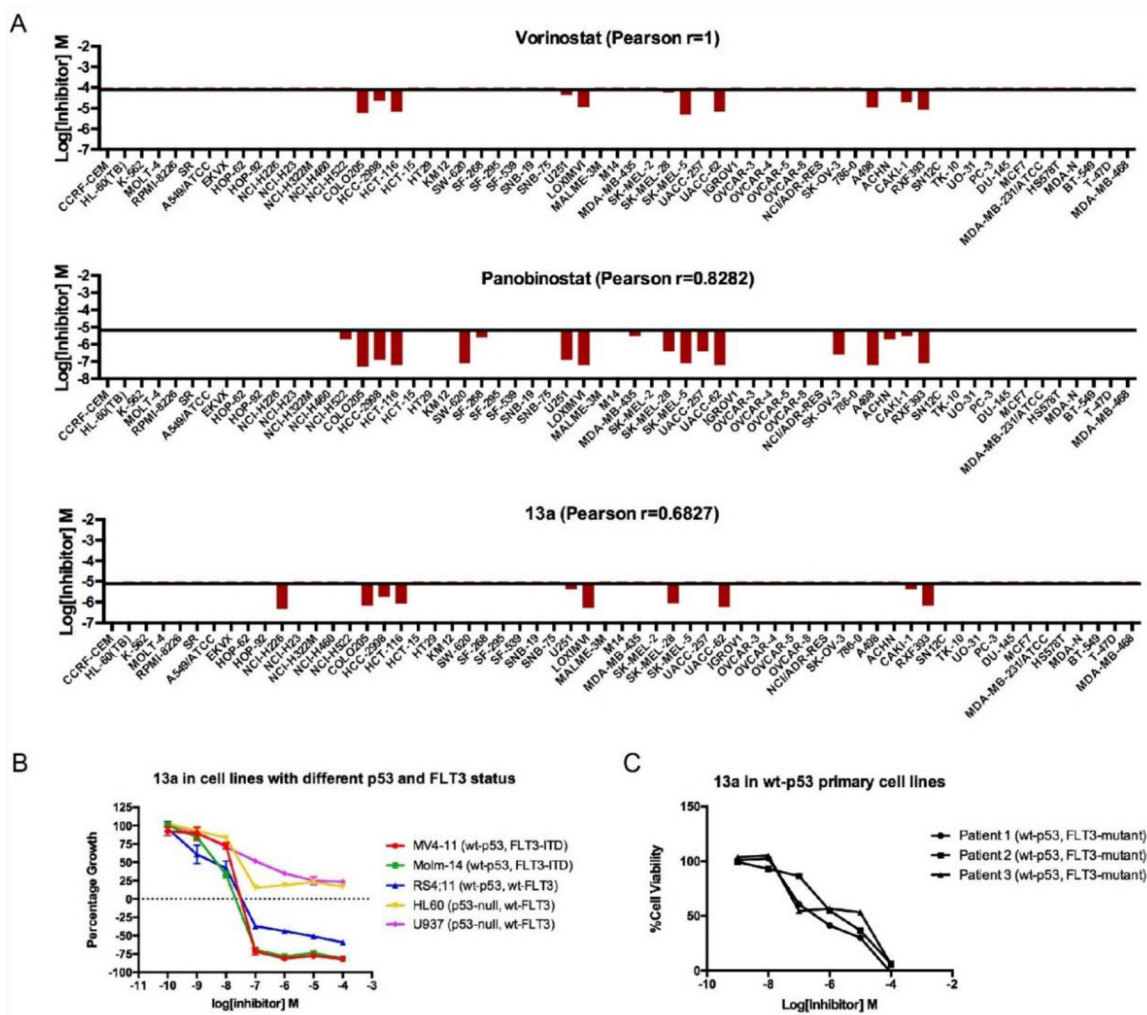
Figure 4A.

NCI 60 cells panel screen of **13a**, panobinostat and SAHA. Compared to panobinostat, **13a** shows better selectivity among all cell lines, and most of the cell lines sensitive to **13a** is p53 wild type. **4B**. In leukemia cells, **13a** is altered due to different p53 and FLT3 status. **3C**. **13a** causes wt-p53 primary cell death. Concentration response curves performed in triplicates were generated using GraphPad Prism software.

Figure 5A.

Treatment of **13a**, LP411, panobinostat (Pan), vorinostat (Vor) and entinostat (Ent) in wt-p53, FLT3-ITD MV4–11 cell line for 24 h. **5B**. (top) Treatment of 200 nM **13a** with 3 h, 6 h, 9 h, 12 h, and 24 h, respectively. LC3-II accumulated within 12 h and is fully degraded in 24 h; (bottom) Quantification of LC3-II values were normalized to actin levels. **5C**. Treatment of **13a**, LP411, panobinostat (Pan), vorinostat (Vor) and entinostat (Ent) in wt-p53, wt-FLT3 RS4;11 cell line for 24 h. **5D**. Treatment of **13a**, LP411, panobinostat (Pan), vorinostat (Vor) and entinostat (Ent) in p53-null, wt-FLT3 HL60 cell line for 24 h.

Figure 6A.

Treatment of **13a** (100 nM) or **13a** (100 nM) in combination with p53-MDM2 inhibitor RG7388 (300 nM) and p53 activator Prima-1met (1000 nM) for 24h, respectively. RG7388 can prevent p53 degradation and promote **13a**-triggered apoptosis obviously; **6B**. Treatment of **13a** (200 nM) and **13a** (200 nM) in combination with RG7388 (300 nM) for 3h, 6h, 9h, 12h and 24h, respectively. p53 begins to degrade after treatment by **13a** for 6h-9h, and the degradation of p53 can be fully recovered by RG7388 within 12h; **6C**. Combination Index (CI) for **13a** and RG7388 after treatment 0f 24 h. Data was analyzed using CompuSyn Software. CI < 1, = 1, and > 1 indicate synergism, additive effect, and antagonism, respectively.
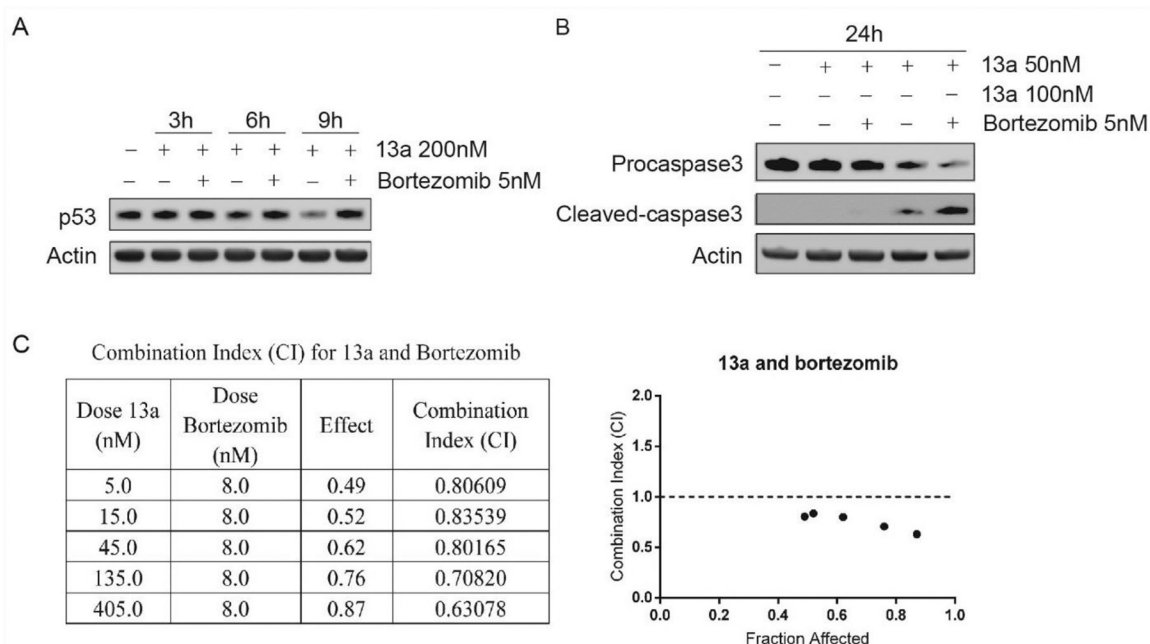
Figure 7A.

Treatment of **13a** (200 nM) or **13a** (200 nM) in combination with bortezomib (5 nM) for 3 h, 6 h and 9 h, respectively. p53 begins to degrade in treatment of **13a** at 6 h, and the degradation can be rescued by bortezomib. **7B**. Treatment of **13a** 50 nM, 100 nM or in combination with bortezomib (5 nM). Bortezomib can promote **13a**-triggered apoptosis. **7C**. Combination Index (CI) for **13a** and Bortezomib after treatment 0f 24 h. Data was analyzed using CompuSyn Software. CI < 1, = 1, and > 1 indicate synergism, additive effect, and antagonism, respectively.
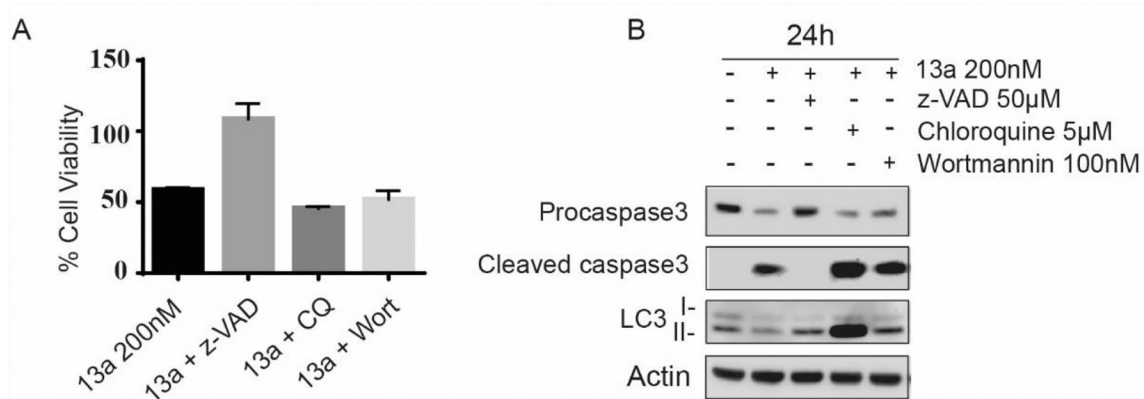
Figure 8A.

Treatment of **13a** (200 nM) with z-VAD (50 μM), chloroquine (CQ 5 μM) or wortmannin (Wort 100 nM) for 24 h incubation (*p < 0.001, n = 3). The pan-caspase inhibitor z-VAD is capable of attenuating cell death rather than the autophagy inhibitors wortmannin and chloroquine, suggesting although both of apoptosis and autophagy occur after treatment of **13a**, apoptosis is the key factor leading to cell death. **8B**. Treatment of **13a** (200 nM) with z-VAD (50 μM), chloroquine (CQ 5 μM) or wortmannin (Wort 100 nM) for 24 h incubation (*p < 0.001, n = 3). z-VAD rescues procaspase activation, and chloroquine blocks the degradation of LC3-II in 24 h and prevent the progression of autophagy.
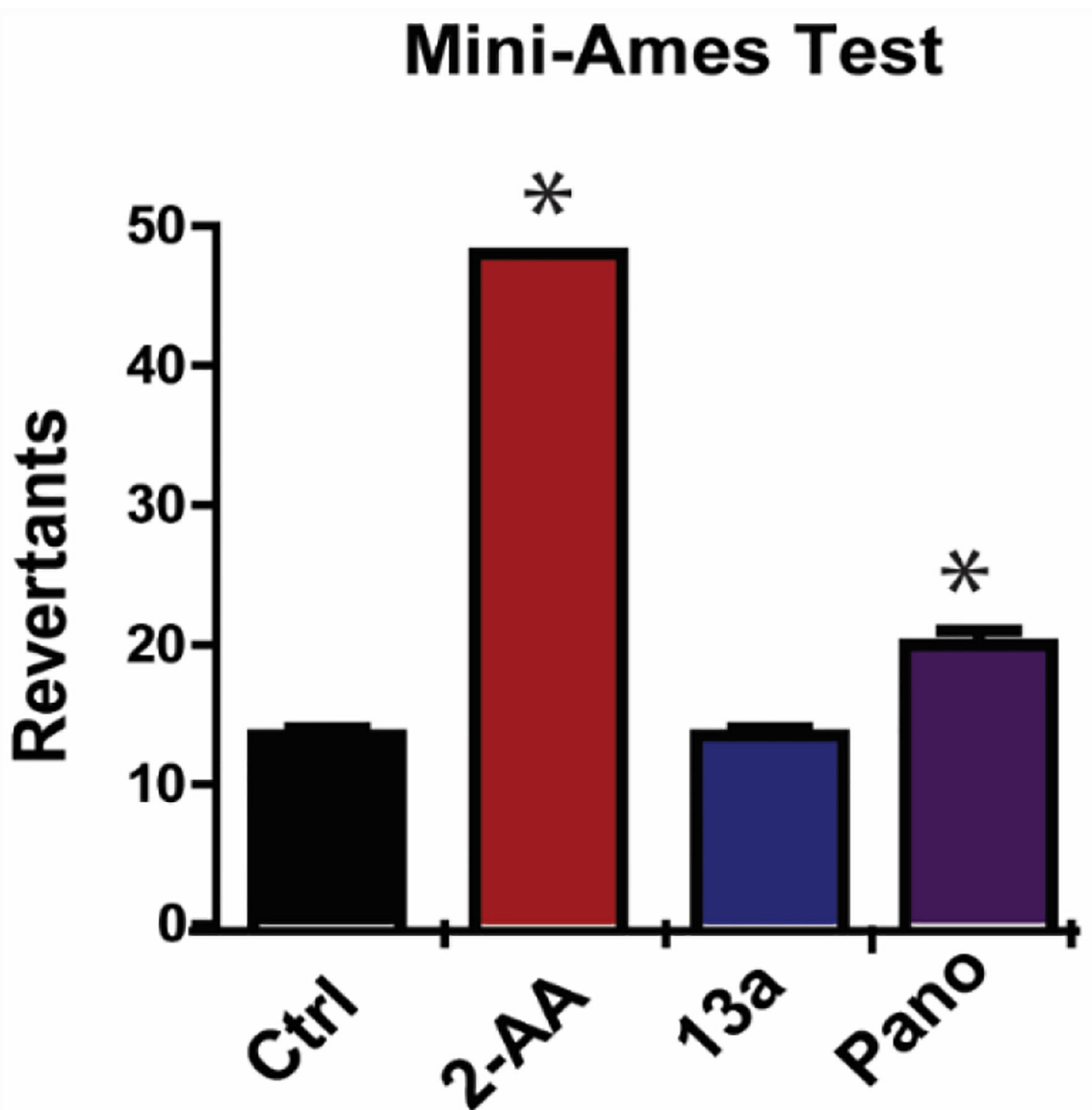
Figure 9.
Mini-Ames tests with liver S9 fraction activation (EBPI, Canada). Mutagen controls 2-aminoanthracene (2-AA) and HDAC inhibitor panobinostat (*p < 0.01 versus Ctrl) are Ames positive. **13a** is not mutagenic as compared to panobinostat and the known mutagen 2-aminoanthracene.
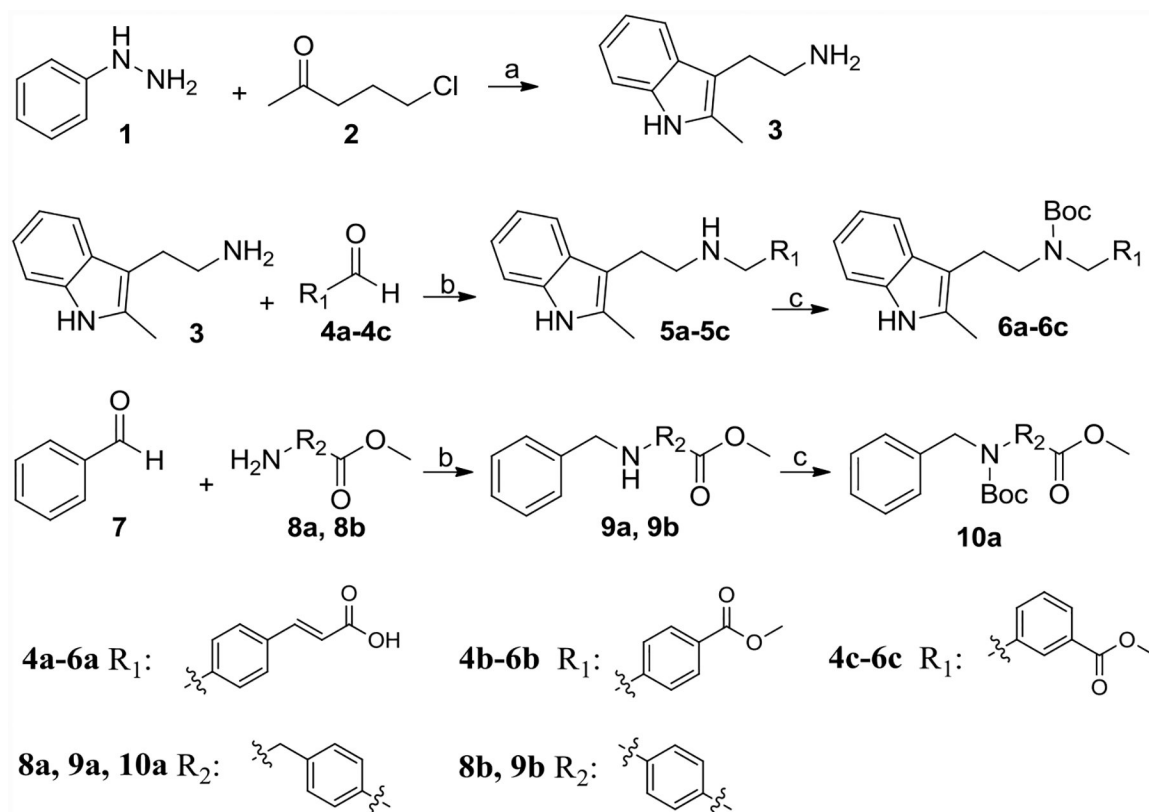
Scheme 1.

Synthesis of **3**, **6a-6c**, **10a** and **10b**.

Reagents and conditions: (a) Ethanol, NaOH, reflux, 47%; (b) NaBH$_3$CN, CH$_3$COOH, methanol, 70–80% yield; (c) Boc$_2$O, TEA, DCM, 80–85% yield; (d) Propionaldehyde or benzaldehyde, NaBH$_3$CN, HCl, Ethanol, 60–70%.
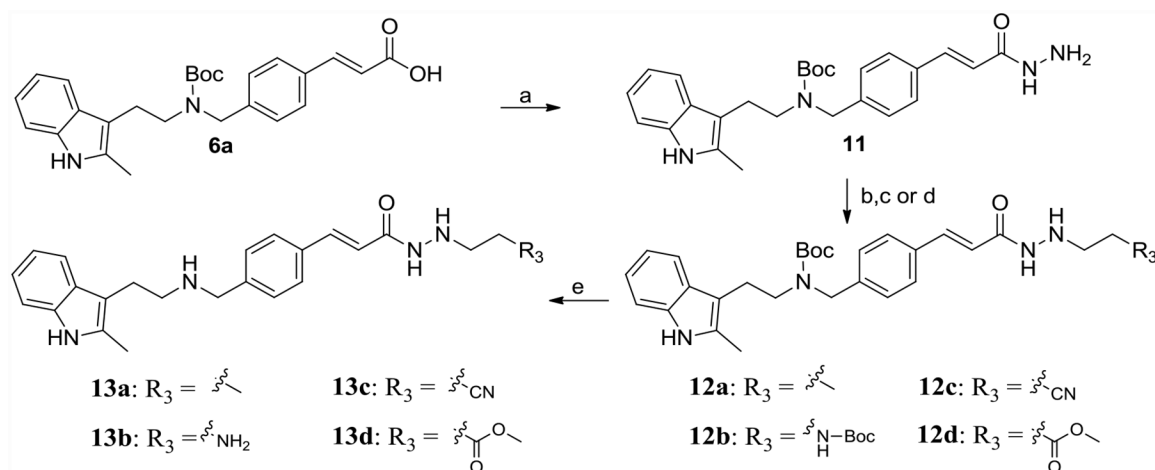
Scheme 2.

Synthesis of **13a**-**13d**.

Reagents and conditions: (a) hydrazine monohydrate, TBTU, TEA, DMF, yield 50%; (b) propionaldehyde or *N*-Boc-2-aminoacetaldehyde, MgSO$_4$, ethanol, yield 60–70%; (c) NaBH$_3$CN, HCl, methanol, H$_2$O, methyl orange, yield 60–70%; (d) acrylonitrile or methyl acrylate, ethanol, refluxed, yield 40–50%; (e) TFA, DCM, yield 60%.
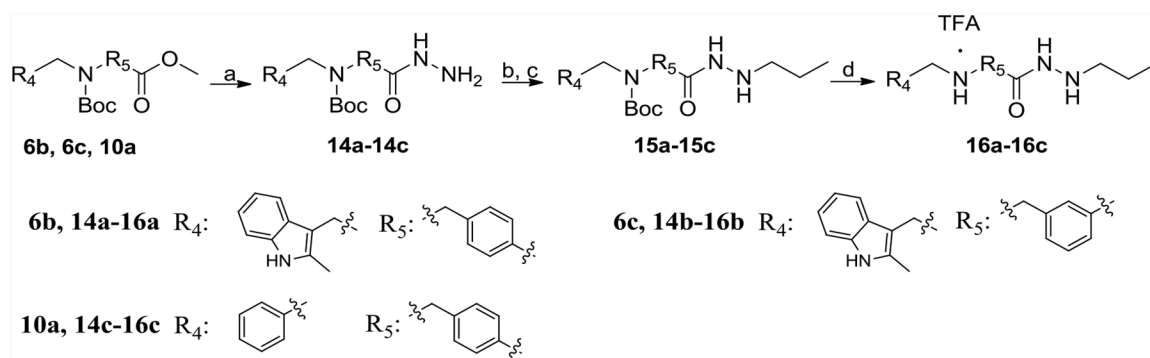
Scheme 3.
Synthesis of **16a**-**16c**.

Reagents and conditions: (a) hydrazine monohydrate, methanol, reflux, yield 90–95%; (b) propionaldehyde, $MgSO_4$, ethanol, yield 60–70%; (c) $NaBH_3CN$, HCl, methanol, H_2O, methyl orange, yield 60–70%; (d) TFA, DCM, yield 60–70%.
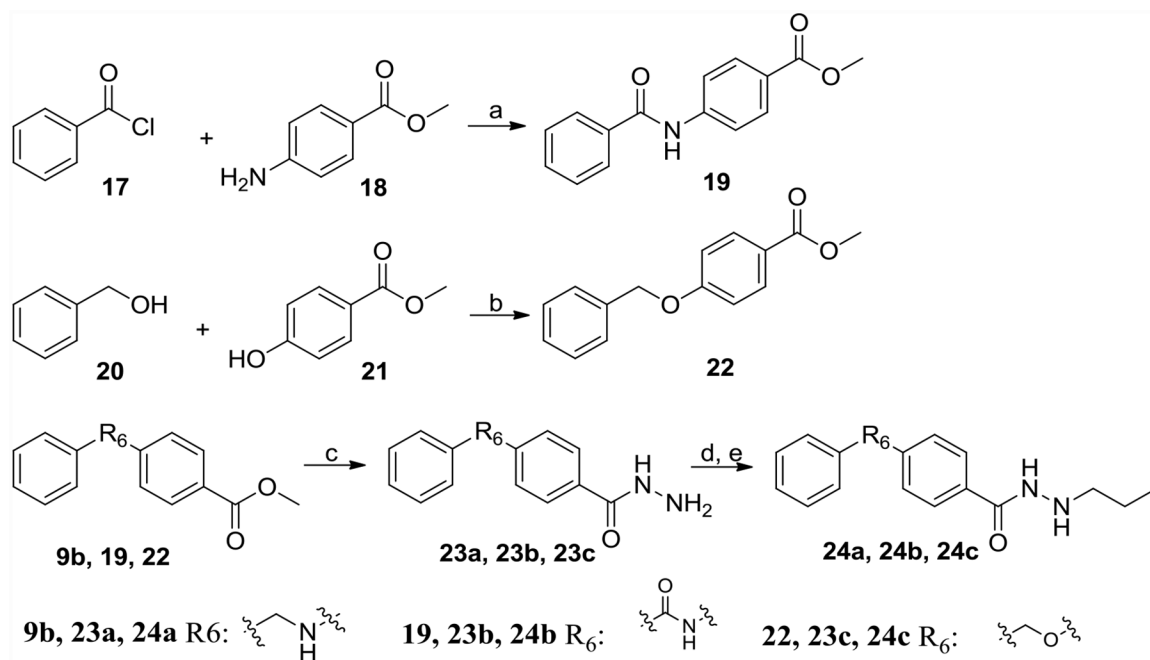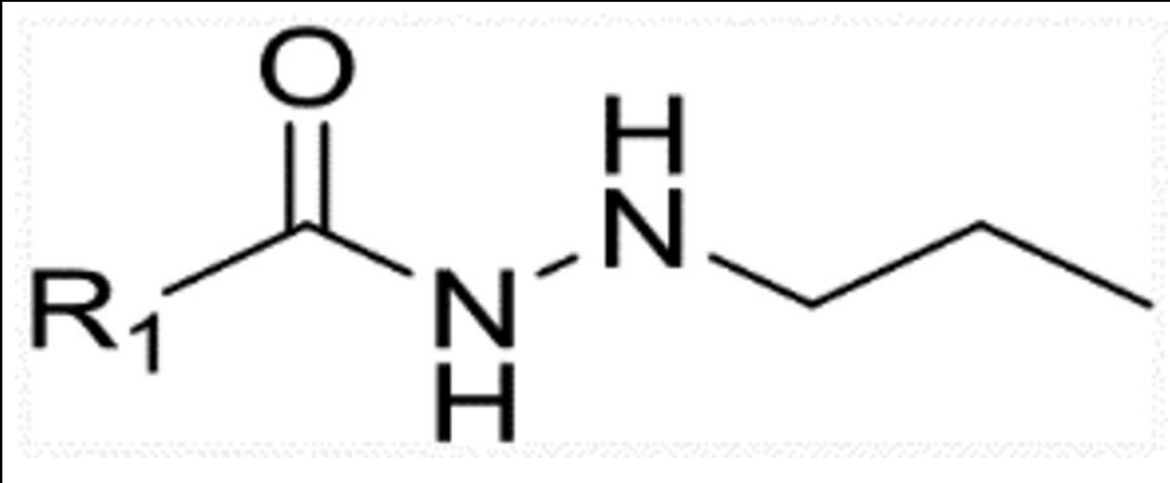
Scheme 4.
Synthesis of **24a**-**24c**.

Reagents and conditions: (a) DCM, TEA, DMF, yield 80%; (b) PPh$_3$, DEAD, anhydrous THF, yield 53%; (c) hydrazine monohydrate, methanol, reflux, yield 95%; (d) propionaldehyde, MgSO$_4$, ethanol, yield 60–70%; (e) NaBH$_3$CN, HCl, methanol, H$_2$O, methyl orange, yield 60–70%.
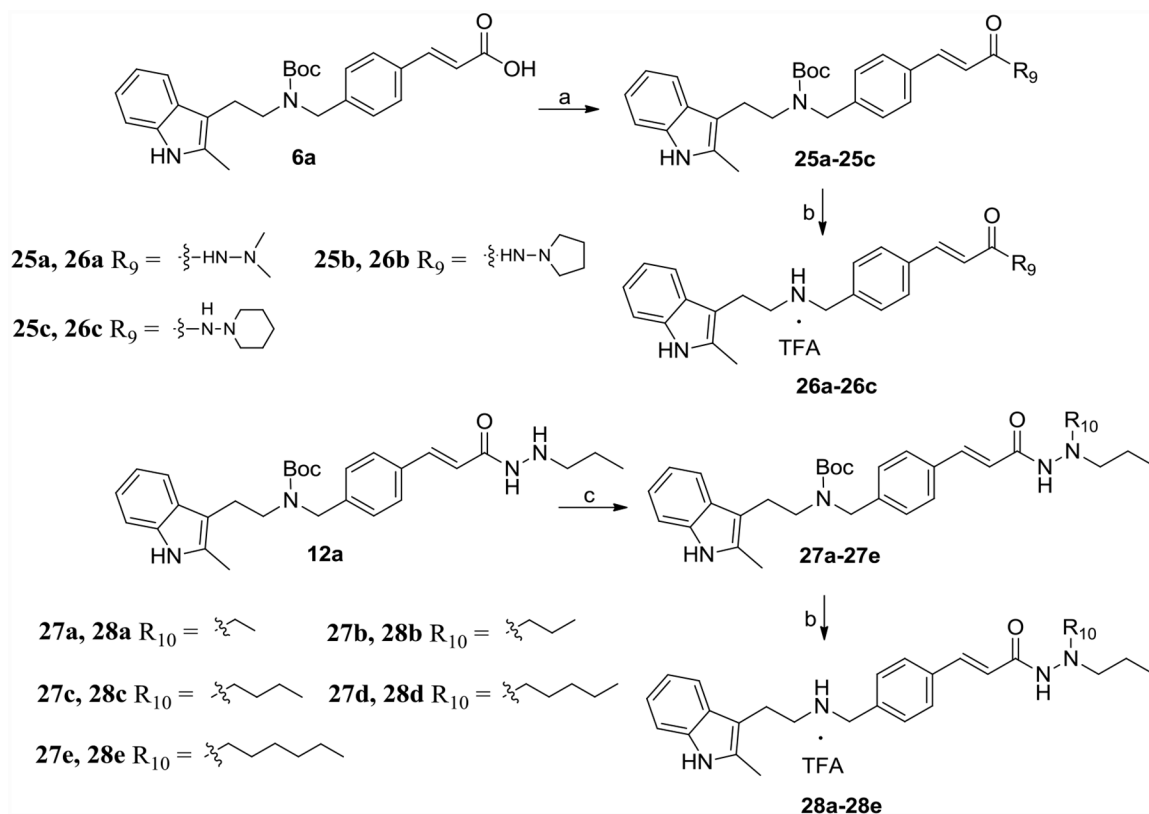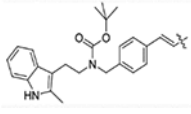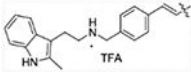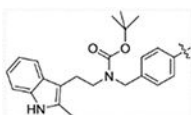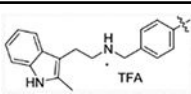
Scheme 5.

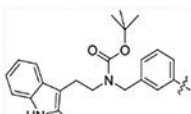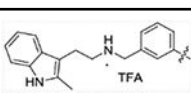Synthesis of **26a-26c**, **28a-28e**.

Reagents and conditions: (a) 1,1-dimethylhydrazine, pyrrolidin-1-amine, piperidin-1-amine or pyrazolidine, TBTU, TEA, DMF, yield 50–60%; (b) TFA, DCM, yield 60–65%. (c) ethanal, propanal, *n*-butanal, *n*-pentanal, *n*-hexanal, NaBH$_3$CN, CH$_3$COOH, methanol, yield 50–60%.
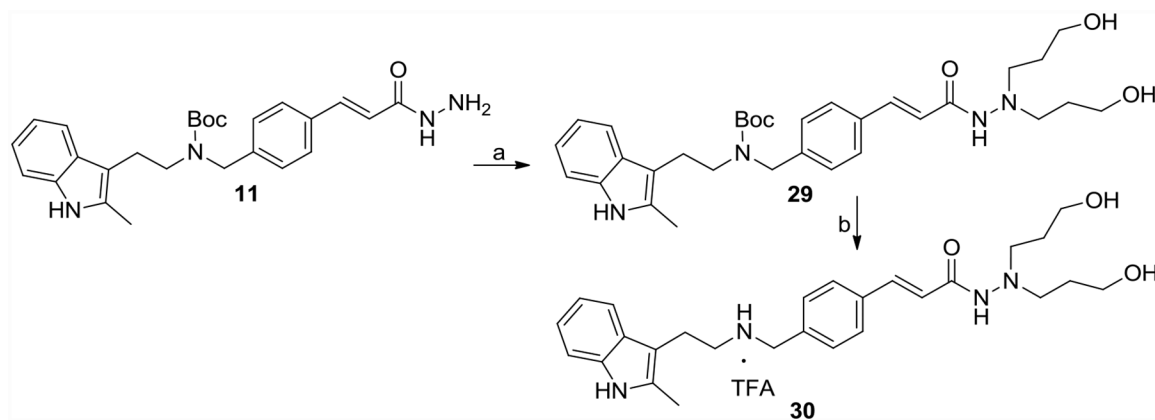
Scheme 6.

Synthesis of **30**.

Reagents and conditions: (a) 3-Bromo-1-propanol, K₂CO₃, ethanol, reflux, yield 70% ; (b)
TFA, DCM, yield 60%.

Table 1.

Structure IC$_{50}$ of compounds in series 1 against HDAC1, 2, 3 and 6.

Compound No.	R$_1$	IC$_{50}$ (nM)[a]			
		HDAC1	HDAC2	HDAC3	HDAC6
12a		180.9	1298	16.76	>50,000
13a		5.17	49.5	0.28	>50,000
15a		28.84	278.6	12.59	>50,000
16a		29.43	107.5	19.94	>50,000
15b		2524	> 5000	> 5000	>50,000
16b		1674	4942	673.9	>50,000
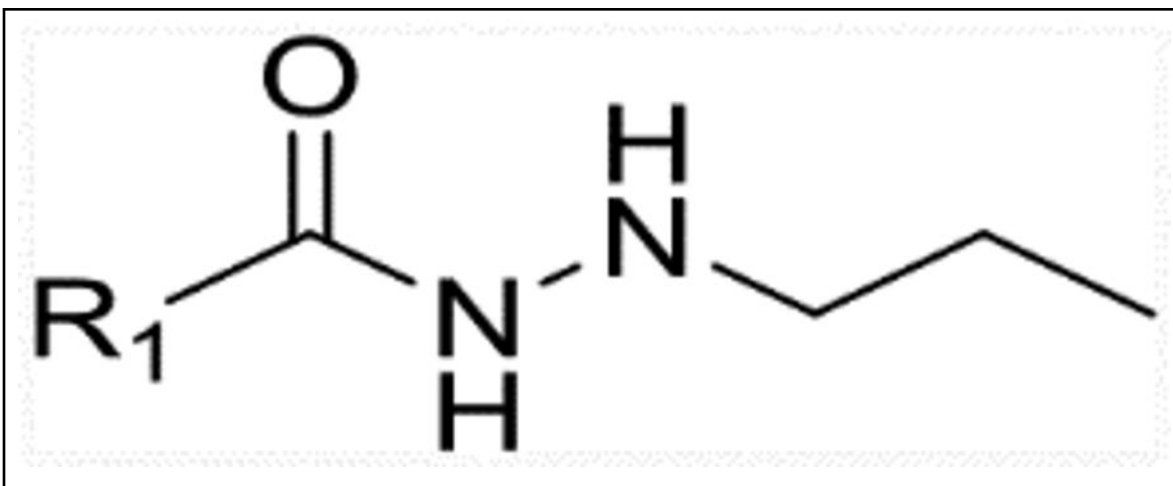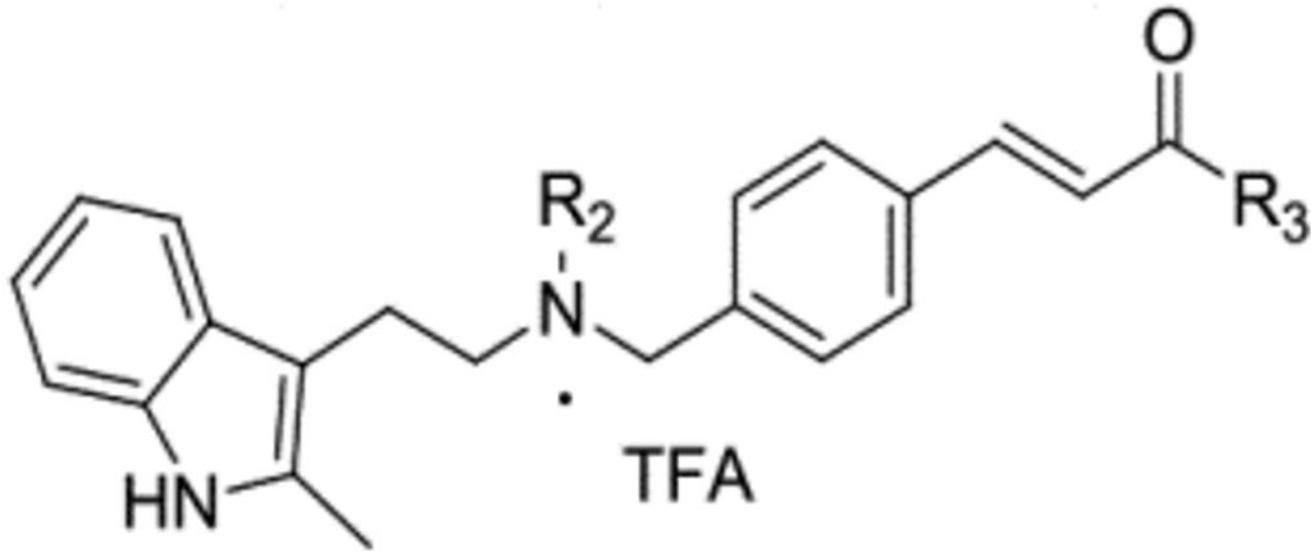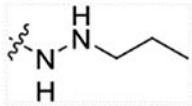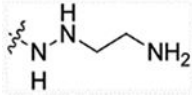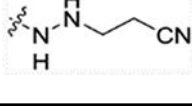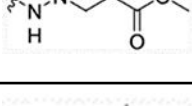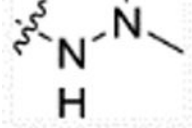
Compound No.	R₁	IC$_{50}$ (nM)^a			
		HDAC1	HDAC2	HDAC3	HDAC6
15c		216.5	579.3	78.14	>50,000
16c		87.98	441.3	96.71	>50,000
24a		15.8	67.48	6.12	>50,000
24b		93.05	474.1	48.75	>50,000
24c		56.32	174.6	24.82	>50,000
Panobinostat		2.5	13.2	2.1	10.5
SAHA		43.76	89.23	144.7	78.3

^{a}Values are average of three independent determinations, the SD values are < 20% of the mean.

Table 2.

Inhibition of HDAC1, 2, 3, and 6 for Compounds in series 2.

	R₂	R₃	IC₅₀ (nM)[a]			
			HDAC1	HDAC2	HDAC3	HDAC6
13a	H		5.17	49.5	0.28	>50,000
13b	H		9842	>10000	5241	>50,000
13c	H		58.12	172	34.82	>50,000
13d	H		1089	4214	309.7	>50,000
26a	H		11000	12930	996.4	>50,000
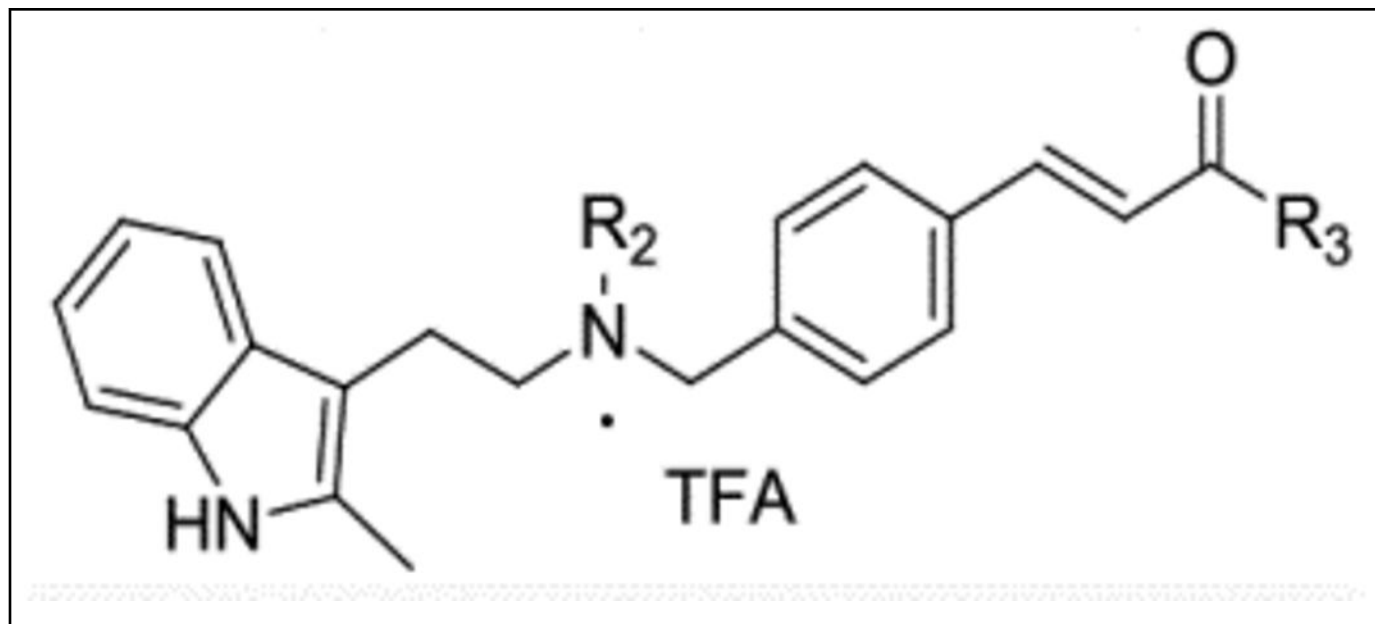
	R₂	R₃	IC₅₀ (nM)[a]			
			HDAC1	HDAC2	HDAC3	HDAC6
26b	H	⌇-HN–N⟨pyrrolidine⟩	8599	>10000	3091	>50,000
26c	H	⌇–N(H)–N⟨piperidine⟩	>10000	>10000	>10000	>50,000
28a	H	⌇-HN–N(propyl)	2925	8071	550.1	>50,000
28b	H	⌇-HN–N(dipropyl)	412.8	1366	25.19	>50,000
28c	H	⌇-HN–N(dibutyl)	209.7	3222	229.4	>50,000
28d	H	⌇-HN–N(dibutyl)	381.5	7316	321.1	>50,000
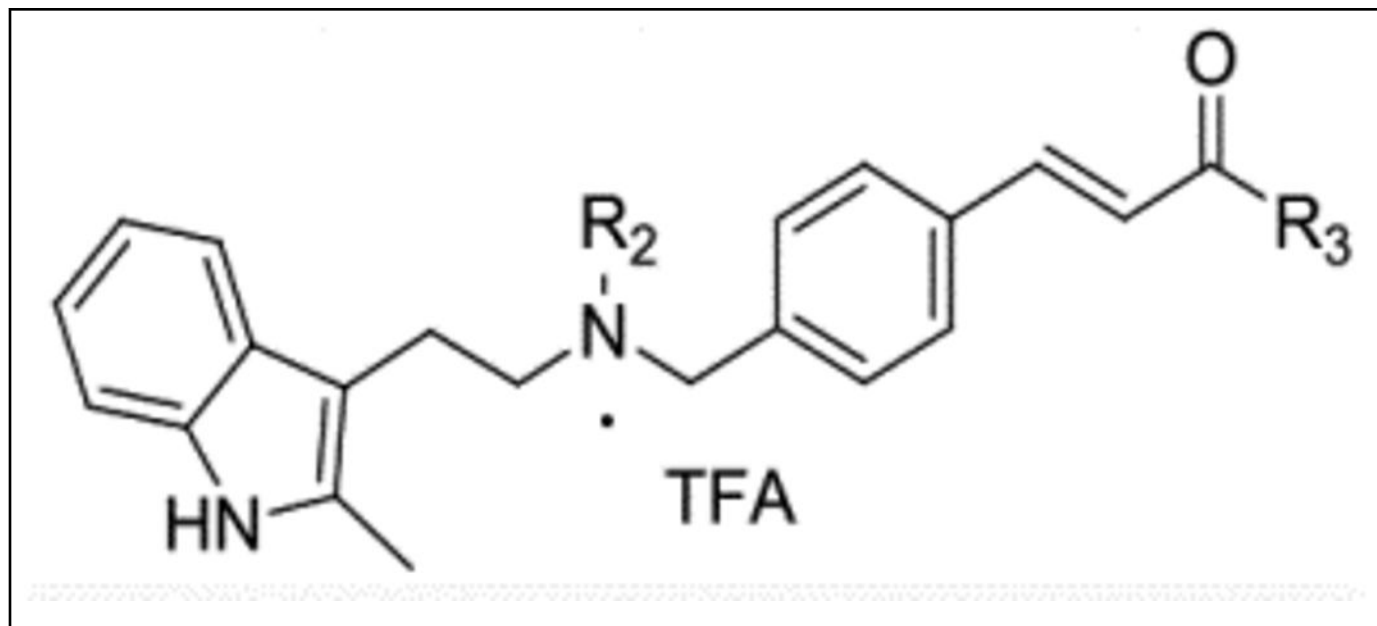
	R₂	R₃	IC₅₀ (nM)[a]			
			HDAC1	HDAC2	HDAC3	HDAC6
28e	H	-HN–N (dipropyl)	2880	9835	143.2	>50,000
30	H	-HN–N (bis-hydroxyethyl)	>10000	>10000	>10000	>50,000

[a]Values are average of three independent determinations, the SD values are < 20% of the mean.

Table 3.

EC$_{50}$ of representative compounds.

Cpd No.	EC$_{50}$[a] (nM) of MV4–11
13a	15.35±2.22
16a	81.64±5.29
16b	7696±1002
16c	172.6±38.75
28b	1054±240.6
Vorinostat	418.1±72.27
Entinostat	806.2±68.72
Panobinostat	5.2±1.87

[a]EC$_{50}$ values were shown as the mean of three experiments ± the standard error of the mean.

Table 4.

IC_{50} of **13a** against HDAC1–9.

HDAC Classes	HDAC isotypes	IC_{50}^{a} of 13a (nM)	IC_{50} of Panobinostat (nM)[65]	IC_{50}^{a} of Entinostat (nM)
Class I	HDAC1	4.69±1.28	2.5	53.89±5.29
	HDAC2	46.0±5.39	13.2	108.2±8.28
	HDAC3	0.28±0.12	2.1	77.18±6.30
	HDAC8	1755±110.2	277	>10,000
Class IIa	HDAC4	>10,000	203	>10,000
	HDAC5	>10,000	7.8	>10,000
	HDAC7	>10,000	531	>10,000
	HDAC9	>10,000	5.7	>10,000
Class IIb	HDAC6	>10,000	10.5	>10,000

^{a}IC_{50} values were shown as the mean of at least three experiments ± the standard error of the mean.

Table 5.

National Cancer Institute Developmental Therapeutics Program *In Vitro* Testing Results of **13a**.

Cancer Types	Cell Line	GI_{50} (nM)	LC_{50} (nM)
Leukemia	CCRF-CEM	40.6	>10,000
	HL-60	34.2	>10,000
	K-562	35.2	>10,000
	MOLT-4	47.7	>10,000
	RPMI-8226	26.8	>10,000
	SR	94.7	>10,000
Non-Small Cell Lung Cancer	A549/ATCC	176	>10,000
	EKVX	285	>10,000
	HOP-62	102	>10,000
	HOP-92	23.0	>10,000
	NCI-H226	52.3	460
	NCI-H23	182	>10,000
	NCI-H322M	173	>10,000
	NCI-H460	163	>10,000
	NCI-H522	96.9	>10,000
Colon Cancer	COLO 205	29.8	660
	HCC-2998	143	1760
	HCT-116	22.9	879
	HCT-15	313	>10,000
	HT29	32.4	>10,000
	KM12	116	>10,000
	SW-620	53.0	>10,000
CNS Cancer	SF-268	198	>10,000
	SF-295	131	>10,000
	SF-539	98.9	>10,000
	SNB-19	231	>10,000
	SNB-75	312	>10,000
	U251	80.1	4280
Melanoma	LOX IMVI	118	537
	MALME-3M	48.2	>10,000
	M14	72.5	>10,000
	MDA-MB-435	97.5	>10,000
	SK-MEL-2	73.9	>10,000
	SK-MEL-28	68.7	893
	SK-MEL-5	192	>10,000
	UACC-257	79.6	>10,000

Cancer Types	Cell Line	GI_{50} (nM)	LC_{50} (nM)
	UACC-62	72.6	589
Ovarian Cancer	IGROV1	115	>10,000
	OVCAR-3	135	>10,000
	OVCAR-4	105	>10,000
	OVCAR-5	31.6	>10,000
	OVCAR-8	41.3	>10,000
	NCI/ADR-RES	516	>10,000
	SK-OV-3	98.3	>10,000
Renal Cancer	786–0	161	>10,000
	ACHN	85.5	>10,000
	CAKI-1	101	4300
	RXF 393	23.4	666
	SN12C	158	>10,000
	TK-10	17.3	>10,000
	UO-31	173	>10,000
Prostate Cancer	PC-3	54.2	>10,000
	DU-145	90.8	>10,000
Breast Cancer	MCF7	106	>10,000
	MDA-MB-231/ATCC	203	>10,000
	HS 578T	121	>10,000
	BT-549	338	>10,000
	T-47D	23.9	>10,000
	MDA-MB-468	50.4	>10,000

Table 6.

Pharmacokinetic characterization of **13a** with iv and oral administration.

Administered dose (mg/kg)	13a iv at 5 mg/kg	13a oral at 20 mg/kg	Panobinostat[93] oral at 50 mg/kg
C_{max} (ng/mL)	--	45.1	116
$t_{1/2}$ (h)	15.2	7.45	2.9
$AUC_{0\text{-}inf}$ (ng·h/mL)	334	265	126
F%	--	19.8	4.62

[a]**13a** was injected via iv and oral (n = 3), blood was sampled at different time-points after dosing for 24 h, and the inhibitor plasma concentration is determined via LC-MS/MS. The area under the plasma concentration versus time curve (AUC) is calculated using the linear trapezoidal method. The PK data are fitted to obtain PK parameters using the non-compartmental method.